Observations of the Interaction and Transport of Fine Mode Aerosols with Cloud and/or Fog in Northeast Asia from Aerosol Robotic Network (AERONET) and Satellite Remote Sensing

T. F. Eck[1,2], **B. N. Holben**[1], **J. S. Reid**[3], **P. Xian**[3], **D. M. Giles**[1,4], **A. Sinyuk**[1,4], **A. Smirnov**[1,4], **J. S. Schafer**[1,4], **I. Slutsker**[1,4], **J. Kim**[5], **J-H. Koo**[5], **M. Choi**[5], **K. C. Kim**[6], **I. Sano**[7], **A. Arola**[8], **A. M. Sayer**[1,2], **R. C. Levy**[1], **L. A. Munchak**[1], **N. T. O'Neill**[9], **A. Lyapustin**[1], **N. C. Hsu**[1], **C. A. Randles**[1,*], **A. M. Da Silva**[1], **V. Buchard**[1,2], **R. C. Govindaraju**[1,4], **E. Hyer**[3], **J. H. Crawford**[10], **P. Wang**[11], **X. Xia**[11]

[1]NASA Goddard Space Flight Center, Greenbelt, MD, USA [2]Universities Space Research Association, Columbia, MD, USA [3]Naval Research Laboratory, Monterey, CA, USA [4]Science Systems Applications, Inc., Lanham, MD, USA [5]Yonsei University, Seoul, South Korea [6]Gwangju Institute of Science and Technology, Gwangju, South Korea [7]Kinki University, Osaka, Japan [8]Finnish Meteorological Institute, Kuopio, Finland [9]Universite de Sherbrooke, Quebec, Canada [10]NASA Langley Research Center, Hampton, VA, USA [11]LAGEO, Institute of Atmospheric Physics, Chinese Academy of Sciences, Beijing, China

Abstract

Analysis of sun photometer measured and satellite retrieved aerosol optical depth (AOD) data has shown that major aerosol pollution events with very high fine mode AOD (>1.0 in mid-visible) in the China/Korea/Japan region are often observed to be associated with significant cloud cover. This makes remote sensing of these events difficult even for high temporal resolution sun photometer measurements. Possible physical mechanisms for these events that have high AOD include a combination of aerosol humidification, cloud processing, and meteorological co-variation with atmospheric stability and convergence. The new development of Aerosol Robotic network (AERONET) Version 3 Level 2 AOD with improved cloud screening algorithms now allow for unprecedented ability to monitor these extreme fine mode pollution events. Further, the Spectral Deconvolution Algorithm (SDA) applied to Level 1 data (L1; no cloud screening) provides an even more comprehensive assessment of fine mode AOD than L2 in current and previous data versions. Studying the 2012 winter-summer period, comparisons of AERONET L1 SDA daily average fine mode AOD data showed that Moderate Resolution Imaging Spectroradiometer (MODIS) satellite remote sensing of AOD often did not retrieve and/or identify some of the highest fine mode AOD events in this region. Also, compared to models that include data assimilation of satellite retrieved AOD, the L1 SDA fine mode AOD was significantly higher in magnitude, particularly for the highest AOD events that were often associated with significant cloudiness.

Corresponding author: Thomas Eck (thomas.f.eck@nasa.gov).
*Now at ExxonMobil Research and Engineering Company, Annandale, NJ, USA

1 Introduction

The largest sources of uncertainty in the anthropogenic radiative forcing of climate are due to aerosol particles, both through direct forcing and also especially their indirect and/or semi-direct effects on clouds (IPCC, 2013). At the same time, severe haze events have their own societal impacts in regard to human health, operations and transportation, and overall quality of life (e.g. Pope, 2000). Identifying and accurately quantifying the various climate and other societal effects of severe haze events has proved difficult both observationally and in atmospheric simulations. Observationally, there are some limitations to the separation of aerosol and cloud properties from passive satellite remote sensing retrievals of aerosol optical depth (AOD) due to cloud contamination of aerosol observations (Zhang et al., 2005; Kaufman et al. 2005; Remer et al. 2013) and due to reflected radiation from the sides of clouds into the aerosol field thereby enhancing the apparent aerosol signal (e.g., the 3-D radiative cloud adjacency effect; Marshak et al., 2008; Varnai and Marshak, 2009). Passive satellite algorithms often identify high concentration aerosol events as clouds and therefore fail to perform AOD retrievals (Shi, 2015). Severe haze events frequently also have stratocumulus cloud elements. Finally, haze events have a high degree of spatial and temporal variability. Ultimately, severe haze events represent the physical continuity between "aerosol particle" and "cloud droplet" including all of the strong nonlinearities associated with aerosol and cloud microphysics, secondary aerosol production, and the overall meteorological environment. Compounding the complexity of the physics is the nature of satellite observing systems themselves and each sensor's strengths and challenges. As shown in studies in Southeast Asia, wide divergences exist in cloud and aerosol products (e.g., Reid et al., 2013) with each observing one limited aspect of the environment. The above issues often make it difficult to accurately observe the near cloud aerosol environment. Vertical profiling observations from lidars may overcome and/or minimize some of these issues but residual cloud contamination may remain, and lidar beams can be completely attenuated in high AOD. Nevertheless, several studies utilized space-borne CALIPSO lidar data (Girolamo et al, 2009; Varnai and Marshak, 2011, and Yang et al. 2012) and aircraft based High Spectral Resolution Lidar (HSRL) data (Su et al. 2008) to investigate aerosol near clouds finding significant enhancements in the vicinity of low altitude clouds.

Models have even more difficulty in coping with severe haze events. Indeed, severe haze in the Indo-Gangetic Plain and in the North China Plain pose the most significant challenging air mass regimes for global aerosol models (Sessions et al., 2015). The models' requirement to resolve shallow moist boundary layer, strong subsidence and stratocumulus clouds coupled with strong nonlinearity in particle hygroscopicity with high relative humidity is daunting. AOD data assimilation only marginally improves the situation, as the input observations and the modeling alike suffer from the same shortcomings as noted above.

Dynamic uncertainties in the model subsequently lessen the impact of data assimilation in forecast time.

For both observations and modeling simulations meteorological co-variation with severe haze can be a particularly difficult issue to accurately quantify due to the possibility of several simultaneous effects such as aerosol humidification in the high relative humidity environment in the vicinity of clouds, cloud processing of existing aerosols (Munger et al., 1986; Noone et al., 1992; Hoppel et al., 1994, Dall'Osto et al., 2009), secondary particle production to sulfate, nitrate, and organic aerosol; (Hansen et al., 1991; Hayden et l. 2008, Ervens et al., 2011). Simulation studies by Quaas et al. (2008) and Grandey et al. (2013a) utilized general circulation models to conclude that aerosol humidification or swelling in high relative humidity regions in the vicinity of clouds was the dominant factor in the model's relationship between AOD and total fractional cloud cover. More recently Gryspeerdt et al. (2016) analyzed satellite data, taking into account cloud droplet number concentration and concluded that the global mean AOD and cloud fraction relationship is reduced by 80% when meteorological co-variation is taken into account. Additionally, increases in aerosols may increase cloud fraction by extending cloud lifetimes as a result of decreasing cloud droplet size, thereby delaying precipitation (Albrecht, 1989).

An early step in assessing the nature of haze events is to determine their probability of formation and then uniformly evaluating the satellite aerosol products and models. From a direct radiative forcing assessment point of view, monitoring the regional ambient aerosol optical state with sun photometers is one way to unambiguously characterize the total integrated atmospheric aerosol column. Due to their small fields of view there is no significant 3-D radiative adjacency effect in sun photometer data when measurements of AOD are made in close proximity to clouds, and the much higher effective temporal resolution, such as from instruments in the Aerosol Robotic Network (AERONET), allows for monitoring of haze evolution throughout the day with much less potential cloud contamination. In sun photometer measurements the small field of view (FOV) insures that the signal is dominated by the direct sun signal with minimal contribution of diffuse radiation (which could originate from cloud multiple scattering) within the field of view. Sinyuk et al. (2012) analyzes the effect of diffuse in the FOV for the AERONET sun-sky radiometers utilized in this study. The spectral deconvolution algorithm (SDA; O'Neill et al., 2003; Kaku et al., 2014), which separates fine and coarse mode AOD, further isolates potential cloud droplets from fine mode particles, including larger haze (cloud processed) particles (Eck et al., 2012). This allows for improvement in the overall observability of the fine mode aerosol system (e.g., Arola et al., 2017).

Aerosol-cloud covariance can come through transport covariance and more "local" cloud effects. For example, transport covariance between significant aerosol outbreaks and synoptic scale frontal cloud features in Asia have been reported (Zhang and Reid, 2009). More interest in the scientific community however has been towards local aerosol-cloud relationships. For example, Zhang et al. (2005) and Jeong and Li (2010) examined satellite and sun photometer derived AODs for marine and continental clouds, respectively. These studies used different algorithms and measurement types (satellite and sun-sky radiometers) to determine what a cloud is, typically by spatial and/or temporal variance (assuming clouds

cause larger variance than aerosols) and not by particle size or chemical composition. The findings of Zhang et al. (2005) suggest that 70% of the increased satellite signal in AOD in the vicinity of marine clouds is due to cloud contamination, with the remaining 30% due to hygroscopicity or secondary production. For clouds in Oklahoma, Jeong and Li (2010) found, from both AERONET sun photometer and aircraft in situ data, enhanced AOD near clouds and that only ~25% of the enhancement was due to humidification, while most was due to the combined effects of new particle formation, cloud processing of particles and convergence of air in clouds. Eck et al. (2012) presented evidence of aerosol growth through cloud processing after the evaporation of extensive fog or low altitude stratus (layer) clouds, with retrieved size distributions from AERONET showing sub-micron mode bimodality similar to that measured by various in situ field measurements. Furthermore Eck et al. (2014) found rapid and sometimes large (doubling at times) increases in fine mode AOD in the immediate vicinity of non-precipitating polluted cumulus clouds from AERONET measurements in the mid-Atlantic USA region. Since there often was no significant change in retrieved particle size or Ångström exponent associated with these increases in AOD, this suggests possible secondary particle production in cloud droplets and/or hygroscopic growth of exiting sub-visible Aitken size particles into the optically effective accumulation mode in addition to hygroscopic growth and cloud processing of existing accumulation mode size particles. Both aircraft in situ and HSRL measurements were consistent with the AERONET measured increases in AOD near these cumulus clouds and additionally consistent in the overall lack of change in fine mode particle size parameters.

Recent research focused on East Asian haze events provides an opportunity for understanding not only their nature, but their observability and predictability as well. During March-June 2012 a regional AERONET field experiment in South Korea and Japan provided an opportunity to investigate remote-sensing signals of aerosol optical properties. In the current paper we analyze the AERONET measurements of AOD during this field campaign in addition to an upwind site in the Northern China Plain (east of Beijing), focusing in particular on the fine mode AOD retrieved by SDA and especially focusing on measurements in the nearby vicinity of clouds or data that were eliminated by cloud screening algorithms. Additionally we examine the retrievals of AOD from satellite by Moderate Resolution Imaging Spectroradiometer (MODIS) sensors from three different retrieval algorithms and compare these to the AERONET retrieved fine mode AOD. Fine mode AOD estimated by aerosol re-analyses (Lynch et al., 2016; Buchard et al., 2015) are also compared to the fine mode AOD from AERONET for selected sites. Finally, we investigate the monthly mean AOD climatology from AERONET at sites in both China and South Korea, specifically analyzing the differences in fine mode AOD from cloud screened versus non cloud-screened data.

This paper primarily analyzes the Version 2 AERONET data that has been utilized in all AERONET data analyses from 2006 through 2016, since the vast majority of the published literature to date have utilized AERONET Version 2 data. The recently developed Version 3 is also examined in the context of relative differences between Version 2 and Version 3 AOD for selected sites and time intervals since the new cloud-screening algorithm is significantly different in Version 3 as compared to Version 2. However more extensive comparisons of Versions 2 and 3 AOD data sets will be the topic of future investigations.

2   Instrumentation, Data and Methodology

For the DRAGON-Korea and DRAGON-Japan 2012 networks, there were 22 AERONET Cimel sun-sky radiometer sites in a meso-scale Distributed Regional Aerosol Gridded Observation Network (DRAGON) in South Korea (11 of these in the greater Seoul metropolitan area) and 14 Cimels in Japan in the spring and summer of 2012 (Sano et al., 2016; Lee and Son, 2016; Holben et al., 2018). These site deployments included existing AERONET long-term monitoring sites in both South Korea and Japan. However, only a subset of these sites were analyzed in detail since many sites were clustered in urban centers (Greater Seoul in South Korea and Osaka in Japan) and therefore showed very similar time series of AOD to each other. Additionally, the occurrence of the field campaign insured that the long-term monitoring stations would be operating well during this time interval.

2.1.1   AERONET Instrumentation

The CIMEL Electronique CE-318 sun-sky radiometer measurements were made with instruments that are a part of the AErosol RObotic NETwork (AERONET) global network. These instruments are described in detail by Holben et al. [1998], however a brief description is given here. The automatic tracking Sun and sky scanning radiometers made direct Sun measurements with a 1.2° full field of view every 15 minutes at 340, 380, 440, 500, 675, 870, 940, and 1020 nm (nominal wavelengths; includes the 1640 nm channel in extended wavelength Cimel versions). It is noted that for this campaign several Cimels were operated with a 3 min sampling interval to obtain higher temporal resolution data, much more frequent than the standard 15 min interval of AERONET. The direct sun measurements take ~8 seconds to scan all wavelengths (repeated three times within a minute), with a motor driven filter wheel positioning each filter in front of the detector. These solar extinction measurements are used to compute AOD at each wavelength except for the 940 nm channel, which is used to retrieve total column water vapor (or precipitable water) in centimeters. The filters utilized in these instruments were ion assisted deposition interference filters with bandpass (full width at half maximum) of 10 nm, except for the 340 and 380 nm channels at 2 nm. The estimated uncertainty in computed AOD, due primarily to calibration uncertainty, is ~0.010–0.021 for field instruments (which is spectrally dependent with the higher errors in the UV; Eck et al. [1999]). Schmid et al. [1999] compared AOD derived from 4 different solar radiometers (including an AERONET sun-sky radiometer) operating simultaneously together in a field experiment, and found that the AOD from 380 to 1020 nm agreed to within a root mean square (RMS) difference of 0.015, which is similar to our estimated level of uncertainty in AOD measurements for field instruments.

For some of the analyses presented, the Version 2 spectral AOD data have been screened for clouds following the methodology of Smirnov et al. [2000], which relies on the higher temporal frequencies of cloud optical depth (COD) as compared to AOD, especially optical depth triplet variability within one minute. Triplet variability is defined as the maximum minus minimum AOD of the three values taken in a one-minute time interval for each wavelength, with all spectral channels being checked for triplet range. AOD measurements pass the Version 2 cloud screening when triplet variability is less than either 0.02 or 0.03*AOD (whichever value is higher) and the measurement is screened if any wavelength

triplet variability exceeds the threshold. In the newer Version 3 cloud screening, only three channels (675m, 870 and 1020nm) are checked for triplet variance, and the measurement is screened when the triplet range for all three wavelengths exceeds 0.01 or 0.015*AOD (whatever is greater). The complete set of Version 3 cloud screening and quality assurance algorithms are provided in another AERONET publication in preparation (David Giles, personal communication). The sky radiances measured by the sun/sky radiometers are calibrated versus frequently characterized integrating spheres at the NASA Goddard Space Flight Center, to an absolute accuracy of ~5% or better [Holben et al., 1998].

2.1.2 Spectral Deconvolution Algorithm (SDA)

Based on the assumption that aerosol size distributions are bimodal, O'Neill et al. (2001; 2003) developed the SDA that utilizes spectral total AOD data to infer the component fine and coarse mode optical depths. An additional fundamental assumption of the algorithm is that the coarse mode Ångström exponent and its derivative are both close to zero, which is based on Mie calculations for coarse mode particles that are assumed to have super micron radii. The Ångström exponent α and the spectral variation of α (as parameterized by $\alpha'=d\alpha/d\ln\lambda$) are the measurement inputs to the SDA. These continuous-function derivatives (computed here at a reference wavelength of 500 nm) are derived from a second order fit of ln AOD versus ln λ (Eck et al., 1999). For purposes of consistency with prior literature, in this study we report the classical AERONET 440–70 nm Angstrom exponent rather than the spectral derivative at 500 nm. The measured spectral AODs employed as input to the SDA were limited to the five CIMEL wavelengths ranging from 380 to 870 nm, and in this study all channels must have been available for the retrievals even though this is not a requirement for Level 2 data. An additional quality control check was utilized in this study to ensure high quality Level 1 data: we only analyzed Level 1 data when Level 2 data were available in the same week. The AERONET data in Level 1 were not screened for clouds, since O'Neill et al. (2003) have shown that SDA incorporates cloud optical depth (COD) into the coarse mode AOD component. Due to far forward scattering by ice, the perceived COD from sun photometry is less than the actual. Nevertheless, the analysis by Chew et al. (2011) of AERONET measured spectral AOD in conjunction with lidar data in Singapore has shown that the SDA technique effectively separated the fine mode AOD component from the total optical depth with a cirrus cloud contamination coarse mode. Additionally, Kaku et al. (2014) have verified that the SDA technique is also effective in separating the fine and coarse modes from in situ spectral optical measurements. However, although the Level 1.0 AOD data do not have the AERONET cloud-screening algorithm of Smirnov et al. (2000) applied, there is still a basic filter of large temporal variance of the signal applied to all Level 1.0 data. The direct sun measurement data are not included in the AERONET Level 1.0 data set if the variance of the raw signal is very high within the triplet sequence. The variance threshold applied is based on the RMS differences of the three direct sun triplet measurements relative to the mean of these three values. If the (RMS/mean)·100% of the triplet values is greater than 16% then the data are not used for computation of AOD and do not appear in the Level 1.0 data set. This temporal variance threshold primarily removes data that are affected by clouds with large spatial–temporal variance in COD. This effectively removes much of the cumulus cloud contaminated data, although some of the thinner edges

with lower COD do remain in the data (see in Eck et al. (2014) the decreases in Ångström exponent in Fig. 6b, and the increases in coarse mode AOD in Fig. 8b, for examples).

The AERONET Level 1 total optical depth uncertainty in the visible and near infrared is ~0.01 after final calibrations are applied and if Level 2 exists for the same time interval. This is the same uncertainty as Level 2 AOD since it is determined primarily by radiometer calibration. The uncertainty in fine AOD in Level 1 data mainly arises from the separation of fine versus coarse mode in the total OD (when thin cloud contaminates the data) or in total AOD when there is no cloud contamination. The definition of the aerosol fine and coarse modes varies between different approaches. For example the Dubovik and King (2000) almucantar retrieval approach defines the two modes as the local minima in size distribution between the two modes (for volume radius ranging from 0.44 to 0.99 micron) while in the O'Neill et al. (2003) SDA algorithm the two modes include the tails of the size distributions with no radius cutoff to define the modes. The fine mode fraction from the SDA is lower than that from the Dubovik retrieval by ~0.05 (Eck et al., 2010) likely due in large part from this difference in definition between modes. Therefore in this paper the high fine mode AOD cases identified by SDA that are screened as clouds by the AERONET algorithms may actually have somewhat higher fine mode AOD as determined by different fine versus coarse mode definitions.

2.1.3 AERONET Inversion Methodology

In addition to AOD from direct sun measurements, the CIMEL collects sky radiance measurements in the almucantar geometry (fixed elevation angle equal to solar elevation, and ±180° azimuthal sweeps) at 440, 675, 870, and 1020 nm (nominal wavelengths). Both types of measurement are used together to retrieve optical equivalent, column integrated aerosol size distributions and refractive indices. Using this microphysical information the spectral dependence of single scattering albedo (SSA) is calculated. The algorithm of Dubovik and King (2000) with enhancements detailed in Dubovik et al. (2006) was utilized in these retrievals, known as Version 2 AERONET almucantar retrievals. Only Version 2 Level 2 quality assured almucantar retrievals (Holben et al., 2006) are presented in this paper, unless otherwise noted. The Version 2 AERONET algorithm determines the percentage of spherical and spheroidal particles required to give the best fit to the measured spectral sky radiance angular distribution. Further details on the Version 2 algorithm and the improved specification of surface bidirectional reflectance can be found in Dubovik et al. (2006) and Eck et al. (2008).

Almucantar sky radiance measurements were made at optical airmasses of 4, 3, 2, and 1.7 (75°, 70°, 60°, 54° solar zenith angle respectively) in the morning and afternoon, and once per hour in between. In order to ensure sky radiance data over a wide range of scattering angles, only almucantar scans at solar zenith angles greater than ~50° are analyzed and presented here. In order to eliminate cloud contamination from the almucantar directional sky radiance data AERONET requires the radiances to be symmetrical on both sides of the sun at equal scattering angles, and symmetric radiances from both sides are subsequently averaged. Directional sky radiance measurements that are not symmetrical (due to cloud on one side or inhomogeneous aerosol distribution) are eliminated, and the minimum number of

measurements required in given scattering angle ranges for a Level 2 retrieval are shown in Holben et al. (2006). The stable performance of the inversion algorithm was illustrated in sensitivity studies performed by Dubovik et al. (2000) where the perturbations of the inversion resulting from random errors, possible instrument offsets and known uncertainties in the atmospheric radiation model were analyzed. Their work employed retrieval tests using known size distributions to demonstrate successful retrievals of mode radii and the relative magnitude of modes for various types of bimodal size distributions such as those dominated by a sub-micron accumulation mode or distributions dominated by super-micron coarse mode aerosols. Although very few direct comparisons of size distribution between in situ and AERONET retrievals have yet been published there are several aerosol types in specific regions that have been or can be compared. For example, Reid et al. (2005) presents a table where the volume median radius of smoke from various major biomass burning regions (South America, southern Africa, and North America (boreal, temperate)) are compared. For all three of these regions, the volume median diameters of the in situ versus the AERONET retrievals are often within ~0.01 μm of each other. Similarly, for fine mode pollution in the Arabian Sea during INDOEX, Clarke et al. (2002) presented lognormal fits of volume size distributions from aircraft and ship in situ instrument measurements that showed average accumulation mode volume peak radius values of 0.17–0.18 μm with geometric standard deviations of 1.43 (aircraft) and 1.51 (ship) for observations made under high aerosol scattering conditions. This compares well with retrievals made at Kaashidhoo Island, Maldives (in the same region), when AOD(440 nm)>0.4, of 0.18 μm median radius and width of 1.49 (AERONET Version 2 averages from 1998–2000). For larger sub-micron sized aerosols, Eck et al. (2010) discussed the relatively close agreement for Pinatubo stratospheric aerosol observations of ~0.56 μm peak volume radius from AERONET retrievals to 0.53 μm effective radius from in situ stratospheric aircraft measurements, as reported by Pueschel et al. (1994). In the coarse mode (super-micron radius), Reid et al. (2006) and Reid et al. (2008) showed excellent agreement between in situ measured size and AERONET retrievals for sea salt and desert dust, respectively. Smirnov et al. (2003) showed reasonable agreement between AERONET retrievals of size distributions and in situ measurements for aerosols of marine origin. Similarly, Johnson and Osborne (2011) have shown good agreement between aircraft in situ measured size distributions and AERONET retrievals for coarse mode dust in the Sahel region of West Africa.

2.2 MODIS Satellite Retrievals of AOD

MODIS is a spaceborne passive imaging radiometer that flies on two satellite platforms: Terra with data from mid 2000 to present and a daytime node Equatorial solar crossing time around 10:30 AM, and Aqua with data from late 2002 to present and a daytime node Equatorial solar crossing time around 1:30 PM as part of the A-Train constellation. The instruments have the same basic characteristics but have aged differently in flight (e.g. Toller et al., 2013, Lyapustin et al., 2014). They measure reflected solar and emitted thermal radiation in 36 bands in the spectral range 412 nm to 14.3 μm, with nominal horizontal pixel sizes at the center of swath from 250 m to 1 km (dependent on band). Due to MODIS' scan geometry and the shape of the Earth pixel sizes become increasingly larger, and shapes distorted, for off-nadir view angles (see Sayer et al., 2015a for the impacts of this so-called 'bow tie effect' on the aerosol products). Several algorithms have been developed and

applied by NASA to provide AOD at 550 nm as part of MODIS routine data processing. A summary of the key features of those used herein is provided below. MODIS data versions are known as 'Collections', each being a full-mission reprocessing for a particular science discipline with consistent algorithms and calibration applied to the whole records to avoid discontinuities. The most recent full Atmospheres discipline reprocessing is Collection 6 (C6); an updated Collection 6.1 (C6.1) reprocessing is ongoing at present, although the cores of the algorithms are similar to those of C6.

2.2.1   Dark Target Algorithm—MODIS Dark Target (DT) consists of two distinct algorithms: one applied over land, and the other over water pixels. The C6 products are described by Levy et al. (2013). In brief, the main data product from both is the AOD at 550 nm; particle size-related information is also provided over water, but not over land, as that aspect of the retrieval was found to have little skill in the latter case. Both land and ocean products are generated with a level 2 pixel size of nominally 10×10 km^2 at the center of the swath. Cloud screening is applied at sensor pixel resolution; after cloud masking, a proportion of additional pixels are discarded, and then the remaining top of atmosphere (TOA) reflectances averaged, with this average spectral TOA reflectance used in the retrieval. Quality assurance (QA) tests use (among other things) the number of such available pixels to assign each retrieval a QA value from 0 (poorest) to 3 (best). Over land it is recommended that only QA=3 retrievals are used, and over water only QA>0 retrievals are used. This QA filtering is applied to create the data set Optical_Depth_Land_And_Ocean that is provided in the aerosol data products, which are denoted MOD04 for data from MODIS Terra and MYD04 for data from MODIS Aqua. The non-QA-filtered equivalent data set is Image_Optical_Depth_Land_And_Ocean. Versions of the DT algorithms have also been applied to Visible Infrared Imaging Radiometer Suite (VIIRS) measurements (Levy et al., 2015).

The over-land DT algorithm is based on the principle that by using shortwave infrared (swIR) bands, where the atmospheric contribution to the TOA signal is dark the surface reflectance in certain visible bands (centered near 470 and 650 nm) can be estimated. This is done using an empirical relationship based on a swIR vegetation index together with Sun/view geometry information (Levy et al., 2007), although the relationship only holds for vegetated surfaces (i.e. dark targets) and so the retrieval is not performed over bright surfaces such as deserts, bare soil, or snow/ice. The AOD at 550 nm is then retrieved by using these surface reflectances and varying the abundances of two aerosol models (both bimodal; one dominated by fine-mode aerosols, with properties dependent on region and season, and the other coarse-mode dominated, to represent mineral dust) in order to match the observed TOA reflectance. The over-water DT algorithm models surface reflectance as a function of near-surface wind speed. Aerosols are modeled by considering combinations between one of four fine mode components and one of five coarse mode components. For each of the resulting 20 fine/coarse mode pairs, the algorithm determines the AOD at 550 nm and a fine/coarse mode aerosol weighting by varying the abundances of these aerosol components to match the observed TOA reflectance. Both best-fit solutions, and the average of all solutions matching the TOA reflectance to within a certain threshold, are provided in

the retrieval products; the latter (average solution) is that which is used in most cases (including here).

The uncertainty of the over-land DT retrievals is expressed as an expected error (EE) envelope in which one standard deviation (around 68%) of retrieved AODs lie relative to the truth. These limits have been established based on validation against AERONET direct-Sun observations (Levy et al., 2013 and Sayer et al., 2014 for C6), and are diagnostic (i.e. defined relative to AERONET). Over land, the EE is of order 0.05+15%, while over water, the envelope is asymmetric and between (−0.02–10%) to (0.04+10%).

2.2.2   Deep Blue Algorithm—A motivation for the original development of Deep Blue (DB) was to fill in gaps in the MODIS DT over-land data products from bright desert/soil surfaces, since these are important source regions for large parts of the global aerosol system, particularly mineral dust (Hsu et al., 2004, 2006). In C6 (Hsu et al., 2013), DB was extended to cover all cloud-free land surfaces (except for snow/ice). Versions of DB have also been applied to Advanced Very High

Resolution Radiometer (AVHRR), Sea-viewing Wide Field-of-view Sensor (SeaWiFS), and VIIRS measurements. The DB retrievals are provided alongside DT in the MOD04/MYD04 aerosol products. A merged DB/DT data set is also provided (Sayer et al., 2014), although this is not discussed here since the aim is to examine the individual algorithms.

The DB algorithm uses different techniques to estimate surface reflectance based on the underlying surface type. For bright surfaces such as deserts, surface reflectance changes comparatively slowly in time and so a surface data base is used. This data base is constructed using a modified version of the minimum reflectance technique, performing a correction for Rayleigh scattering and an assumed background aerosol level, and aggregates observations from over both MODIS records. The data are then binned by season, scattering angle, and normalized difference vegetation index (NDVI) to create data bases at 0.1° horizontal resolution for the MODIS bands centered near 412, 470, and 650 nm (Hsu et al., 2013). The physical principle behind the retrieval is that some 'bright' surfaces such as deserts are in fact comparatively dark in the blue spectral region. Thus the `deep blue' band (412 nm), which gives the algorithm its name, is used to retrieve the AOD at that wavelength. The 470 nm band is used to provide additional retrieval of AOD at 470 nm. These are used together to provide AOD at 550 nm and Ångström exponent, although if the 470 nm AOD is below 0.2 then the Ångström exponent is set to a fixed value and only AOD is retrieved. If internal tests indicate the presence of heavy mineral dust in a pixel, then the 650 nm band is also used and aerosol SSA is retrieved using a maximum likelihood method to pick between one of a candidate set of SSA spectral shapes (Hsu et al., 2013). Over vegetated surfaces, the assumption that surface reflectance varies slowly in time is not valid. In these cases the algorithm uses empirical spectral/directional relationships between the swIR and visible bands (using the same physical principles as the DT approach), and instead uses the 470 and 650 nm bands to retrieve AOD at 550 nm and Ångström exponent.

Aerosol optical properties are set based on region and season, and are the same for both the bright and dark surface algorithm paths. A key difference between DT and DB is that DT

averages cloud-free reflectances within the 10 km retrieval pixel and then does a retrieval, while DB retrieves on each suitable cloud-free 1 km pixel and then averages the retrieved AOD and Ångström exponent to the 10 km grid. Thus, it is possible for a 10 km retrieval pixel to contain inputs from both the bright and dark surface methods. DB also has QA tests (based on pixel availability within the 10 km pixel and its neighbors, and the variability of the retrieved AOD field within the pixel). All retrievals are provided within the data set Deep_Blue_Aerosol_Optical_Depth_550_Land but in most cases it is recommended only to use QA=2 or QA=3 retrievals, which are used to populate Deep_Blue_Aerosol_Optical_Depth_550_Land_Best_Estimate; both are used in this analysis. It is important to note that QA tests and definitions are not the same between DB and DT land or ocean algorithms, despite the common nomenclature.

The C6 DB retrievals have also been validated (Sayer et al., 2013, 2014 for Aqua, Sayer et al., 2015b for Terra). The usual quoted global average EE is 0.03+20%, although prognostic uncertainty estimates have been developed and are included on a pixel-level in the MODIS aerosol data products. Generally errors are smaller over vegetated surfaces than arid ones, and (slightly) smaller for MODIS Aqua retrievals than MODIS Terra (Sayer et al., 2013, 2015b). There is at present no DB over-water data set provided within the MODIS aerosol product distribution.

2.2.3.   MAIAC Algorithm—The Multi-Angle Implementation of Atmospheric Correction (MAIAC) algorithm uses a physical atmosphere-surface model where the model parameters are defined from measurements (Lyapustin et al., 2011a,b; 2012a,b). Instead of swath-based processing, MAIAC starts by gridding MODIS L1B measurements to a fixed 1km grid, and by accumulating a time series of data for up to 16-days using a sliding window technique. This allows MAIAC to observe the same grid cell over time, helping separate atmospheric and surface contributions with the time series analysis and characterize surface bi-directional reflectance distribution function (BRDF) using multi-angle observations from different orbits. Besides BRDF retrieval, the fixed (gridded) surface representation allows characterization of unique surface spectral, spatial, thermal etc. signatures for each 1 km grid cell, helping to improve cloud and snow detection, aerosol retrievals, and atmospheric correction (AC).

Similarly to the DT method, MAIAC uses MODIS swIR (2.1 μm) measurement to predict surface reflectance at 470 nm, with AOD retrieval based on matching the measured TOA reflectance. However, the spectral ratio of surface reflectance between these two bands is defined from measurements using a modified minimum reflectance method, rather than using a statistically averaged empirical spectral/directional relationship as DT does. Over bright surfaces, aerosol retrieval additionally uses a green band (550 nm).

Currently, MAIAC uses eight different regional aerosol optical models over land globally. Smoke/dust detection is synergistic with MAIAC's cloud mask, helping to retain high-contrast fire smoke plumes at 1km resolution in the AOD product with minimal cloud leakage, and also helping to select the proper optical model for the AOD retrieval.

MAIAC reports AOD at gridded 1km resolution at two wavelengths, 470 nm where the original retrieval is made, and interpolated at 550 nm based on the selected aerosol model. The 550 nm value was added for compatibility with the standard AOD products, as well as to support modeling and application analysis commonly using this wavelength. The AOD accuracy is generally similar at the two wavelengths, though it is slightly higher at 470 nm. Along with AOD, MAIAC provides prognostic uncertainty as a function of surface brightness which is modulated by the view geometry, and the QA flag mostly indicating proximity to detected clouds or snow. The recommended QA values are 0 and 1 to obtain the best quality AOD.

The MAIAC MODIS Collection 6 (with enhanced calibration (C6+) which added polarization correction of MODIS Terra, removed residual trends of both Terra and Aqua, and cross-calibrated Terra to Aqua; (Lyapustin et al., 2014) re-processing started in September 2017 using the MODIS Adaptive Processing System (MODAPS). It is expected to be completed in 4–6 months creating a new MODIS product MCD19 accessible via Land Product Distributed Active Archive Center (LP DAAC). Several studies are currently conducting global evaluation of MAIAC AOD. Regional AERONET-based validation over North and South America is available from Superzinsky et al. (2017) and Martins et al. (2017) respectively.

2.3 Data Assimilation Models

2.3.1 NAAPS Model—In this analysis we make use of the Navy Aerosol Analysis and Prediction System-Reanalysis (NAAPS-RA, Lynch et al., 2016). This reanalysis is based on the operational version of NAAPS (http://www.nrlmry.navy.mil/aerosol/), run at the US Navy's Fleet Numerical Meteorological and Oceanographic Center (FNMOC), but with more consistent meteorology, source/sink, and data assimilation procedures throughout the reanalysis time. Four mass-based aerosol source species and one gas species are included in the model, including sea salt, dust and biomass burning. A combined anthropogenic and biogenic fine (ABF) species is run with SO_2 to account for the complex and often collinear behavior of sulfate, organic species, and black carbon species. Smoke from biomass burning is derived from near-real time satellite based thermal anomaly data used to construct smoke source functions (Reid et al., 2009), with additional orbital corrections on MODIS based emissions. Dust is emitted dynamically (Westphal et al., 1989) and is a function of modeled friction velocity to the fourth power, surface wetness and surface erodability, which is adopted from Ginoux (2001) with regional tuning. Sea salt modeling is the same as Witek et al. (2007) and sea salt emission is driven dynamically by sea surface wind. The reanalysis is run offline from a 1°x1° latitude-longitude resolution at 30 levels truncation of the Navy Global Environmental Model (NAVGEM, Hogan et al., 2014). The satellite-derived NOAA Climate Prediction Center (CPC) MORPHing (CMORPH, Joyce et al., 2004) precipitation is used to constrain aerosol wet removal within the Tropics (Xian et al., 2009). A fused AOD product of specially derived and corrected quality controlled MODIS level 3 C5 data (Zhang and Reid, 2006; Hyer et al., 2011) and likewise MISR AOD data (Shi et al., 2014) are assimilated via the Navy Atmospheric Variational Data Assimilation System (NAVDAS) for Aerosol Optical Depth (NAVDAS-AOD; Zhang et al., 2008). The overall correlation between NAAPS reanalysis and AERONET observations is comparable to that of the

satellite aerosol products themselves (Zhang et al., 2008; Lynch et al., 2016). The reanalysis also reproduces the decadal AOT trends found using standalone satellite products in other studies (Lynch et al., 2016).

2.3.2   MERRAero—The MERRA Aerosol Reanalysis (MERRAero; Buchard et al. 2015, 2016) is an offline aerosol reanalysis in which bias-corrected MODIS AOD is assimilated into a version of the NASA Global Earth Observing System, version 5 model (GEOS-5). As described in Buchard et al. (2015), for MERRAero, GEOS-5 is run in "replay" mode, in which a previous meteorological analysis is used to adjust the model's state (winds, temperature, specific humidity), much like in a chemical transport model (CTM), but with aerosol transport dynamics that are consistent with the model's thermodynamic state. In MERRAero, GEOS-5 is replayed from meteorology from the Modern-Era Retrospective Analysis for Research and Applications, version 1 (MERRA-1; Rienecker et al., 2011). The Goddard Chemistry, Aerosol, Radiation and Transport Model (GOCART; Chin et al., 2002; Colarco et al, 2010) is coupled to GEOS-5 to simulate the sources, sinks and chemistry of 15 externally mixed aerosol mass mixing ratio tracers (5 dust bins, 5 sea-salt bins, hydrophobic and hydrophilic black and organic carbon, and sulfate). Then, by means of AOD analysis splitting (see Randles et al., 2017 for technical details), MERRAero assimilates bias-corrected AOD observations from MODIS (both Terra and Aqua, C5 version). The bias-correction algorithm uses a neural network to cloud-screen, homogenize, and translate MODIS reflectances into AERONET-calibrated AOD. This post-processing of the MODIS observations helps to reduce biases in the AOD assimilation relative to independent AOD observations, as shown by Saide et al. (2013). MERRAero Aerosol Absorption Optical Depth (AAOD) and Aerosol Index (AI) were validated with independent observations from the Ozone Monitoring Instrument (Buchard et al., 2015), and PM2.5 were validated with ground observations from the Environmental Protection Agency (Buchard et al., 2016).

3   Results

3.1   Cloud Screening of Fine mode Aerosol Events – Daily averages

In this section we examine large magnitude fine mode AOD events and the cloud screening of some of these events that are associated with extensive cloud cover environments. We will first examine the impacts of Version 2 cloud screening, and then compare with the new Version 3. The AERONET Version 2 database SDA fine mode AOD Level 1 (no cloud screening) versus Level 2 (cloud screened) daily average AOD comparisons for four sites for winter-summer 2012 are presented in Figure 1. Version 2 cloud-screening of AOD data (L2) eliminates many major fine mode AOD events (primarily pollution events) with high AOD (500 nm) > 1.0 at several sites in this East Asian region, including Yonsei University, South Korea, Baengnyeong, South Korea, XiangHe, China, and Fukuoka, Japan (red diamonds without a corresponding black bar, shown in Figure 1). Many of these high fine mode AOD days that were cloud-screened have very few observations of AOD per day (typically due to high cloud fraction seen at MODIS overpasses). Note that some of these AOD observations sometimes pass the Version 2 cloud-screening algorithm, and therefore reach Level 1.5. However, the Version 2 database quality control criteria require that a minimum of 3 AOD

observations per day pass the temporal variability thresholds (AOD one minute triplet range and daily time series checks for temporal spikes; Smirnov et al. 2000) to reach Level 2.

At all of these sites, many of the Level 2 screened high AOD fine mode dominated days comprised a significant percentage of the total number of days when AOD at 500 nm exceeded 1.0. For example, at the Xianghe, China site 4 of the 5 days where daily average fine mode AOD at 500 nm exceeded 2.0 were cloud screened in Version 2 (see Figure 1c). The Ångström Exponent (440–870 nm) for these four cloud screened days ranged from 0.62 to 1.14 and the fine mode fraction of AOD at 500 nm from 0.62 to 0.97. This suggests that many major particulate air pollution events are often associated with extensive cloud cover. However, time interval averaging that yields similar L1 and L2 fine mode AOD values does not necessarily mean that some major aerosol events were not eliminated by cloud screening in the Version 2 data. For example at the Gwangju GIST site (Feb 29-Aug 27, 2012) some high AOD events (>1) are eliminated by L2 cloud screening (see Figure 2). However some low AOD fine mode events are also eliminated by cloud screening, when cirrus clouds occurred with an underlying low AOD layer (see July 15 for example). As a result the ~6 month mean AOD averages for this site are very similar (within ~0.01) for L1 and L2 even though several large fine mode AOD days were eliminated by the cloud screening.

Additionally, we attempt to determine how much influence the missing high AOD days in L2 have on the differences in time interval average values for one site. For the Yonsei site (Figure 3) we compare the L1 and L2 fine mode AOD data for only those days when both levels have a daily mean value. For January through May 2012, for this day-matched data set the fine mode AOD at 500 nm was 0.028 lower for cloud-screened data (L2) versus non-cloud screened (L1). However the AOD was 0.068 lower in L2 than in L1 when all dates where averaged, including days when cloud screening eliminated days with high level pollution AOD (but very few observations). Therefore for this site and time period ~60% of the higher fine mode AOD in the non-cloud screened data ($100 \times (0.068 - 0.028)/0.068$) is due to the cloud screening eliminating days of high aerosol loading events. The remaining increase in AOD in L1 for matched days is mainly due to high variability of AOD in the near vicinity of clouds that is eliminated by L2 screening (see Eck et al, 2014 for this phenomenon in the vicinity of cumulus clouds). High temporal variability of fine mode AOD near to clouds may be due to the turbulent and dynamic physical and chemical environment often associated with clouds, especially cumulus. The relative differences in extended time interval averages (months) for L1 versus L2 fine mode AOD for time matched days only versus all days vary widely between sites; for instance, time interval average differences for all days included are minor for the Gwangju GIST site (Figure 2), but large and significant differences are seen for the Xianghe site.

Now we examine a selected data example to compare the cloud screening of Version 3 with Version 2. The AERONET DRAGON_Korea_Univ site was located in central Seoul and during the time period from May 27–31, 2012 there was a major aerosol event with fine mode AOD levels exceeding 1.0 at 500 nm throughout this 5-day period. Some of these days also had high cloud fraction as seen in MODIS Terra and Aqua images (see Fig. 4b and 4c). The AERONET Version 2 automated cloud screening (Level 1.5 data) resulted in screening of all but 1 or 2 observations on the three days that had the highest AOD of this interval from

May 28–30 (Figure 4a). Since these three days had less than the minimum number of AOD observations per day (three) required for Level 2 there were no AOD data for these 3 days in the Level 2 database. Similar cloud screening occurred for the Yonsei University site (See Figure 1a) on these same dates as both sites are located in Seoul, as well as similar time series for the other nine sites located in the greater Seoul region during this major pollution event. However the new Version 3 cloud screening passed multiple AOD observations for all three of these days (ranging from 6 to 33 points per day; Figure 4), resulting in more complete monitoring of this major aerosol pollution event (average Ångström Exponent (440–6870 nm) of 1.21). This difference in cloud screening is largely due to the change in triplet variability tests (cf. Section 2.1.1). At the longer wavelengths the fine mode AOD decreases rapidly with increasing wavelength, while coarse mode AOD and/or cloud droplet optical depth is nearly constant with wavelength, therefore the triplet variance at longer wavelengths is more attributable to super-micron particle/droplet variation (cloud or dust). In other words, the fine mode fraction of AOD decreases as wavelength increases, as shown in Eck et al. (2010). The average fine mode fraction of AOD at 500 nm was 0.95 over this 5-day interval, from V3 Level 2 daily average data as computed from SDA, therefore obviously a fine mode aerosol dominated event (as also suggested by the high Ångström Exponent). Version 3 cloud screening also has a check for Ångström Exponent (440–870 nm), and if it exceeds 1.0 for an instantaneous measurement then even small numbers of such AOD observations per day are retained in Level 2 database. This case clearly illustrates the enhanced effectiveness of the Version 3 cloud screening and quality assurance (QA) algorithms in correctly identifying fine mode aerosol cases. Version 2 cloud screening clearly at times misidentified fine mode aerosol variability for cloud contamination, resulting in rejection of the data.

A comparison of cloud-screened versus non cloud-screened daily average fine mode AOD from SDA for Version 3 data at the Yonsei University site is shown in Figure 5. This is the same site and time period as shown in Figure 1a (above) for the Version 2 data and can be compared for the differences in cloud screening in Versions 2 and 3. Note that some high AOD days that were cloud screened in Version 2 are not cloud screened in Version 3. Notably, high fine mode AOD days on January 25 and May 28–29 reach level 2 in Version 3 but are screened from Level 2 data in Version 2. On the other hand, the high fine mode AOD day on day 114 (April 23) is screened from Version 3 as cloud, while these data pass the Version 2 cloud screening checks. Note that there is a cloud-screening check in Version 3 for cirrus that does not utilize temporal variance for cloud detection as in Version 2. Instead it relies on independent measurements of sky radiance in the solar aureole as a means of identifying cirrus clouds. If the angular slope of the sky radiance is steep there likely are cirrus cloud crystals present (due to very strong forward scattering) and there is a threshold on this angular dependence for determining cirrus presence. However in this case differences in temporal variance checks (triplets and data spike filter) and differences in the thresholds of the number of observations per day resulted in elimination of the data in Version 3 while it was retained in Version 2. In fact for this day there were 12 observed AOD spectra that passed the V3 temporal variance cloud screening checks but since the Ångström Exponent was less than 1 (~0.8–0.93), this was below the minimum number of points (13) required for the day (minimum 10% of total possible measurements). Lidar data from nearby Seoul

National University showed no directly overhead cirrus present at this time on this day. The two days where both Version 2 and Version 3 screen high AOD events as cloud (February 22 and March 22) seem to have cirrus cloud overlaying an aerosol layer and are screened from Level 2 in both Versions 2 and 3, therefore the only way to detect these high fine mode AOD events when utilizing AERONET data is from SDA Level 1 (non cloud-screened) retrievals.

It is noted that simulation studies of cirrus clouds overlying an aerosol layer (Smirnov et al., 2018) show that the SDA algorithm may underestimate the fine mode AOD by ~5% to ~25% (depending on cirrus crystal size, cirrus optical depth and AOD magnitude). For cirrus crystal size similar to that retrieved by MODIS Collection 6 data for all latitudes, ~30–35 micron effective radius (Yi et al., 2017), this study suggests that the SDA underestimate of fine mode AOD may be on the order of ~10% to 15%. Therefore for these particular high fine mode AOD days with overlying cirrus at the Yonsei University site, the actual fine mode AOD may have been somewhat higher than the already high fine mode AOD retrieved by the SDA algorithm (SDA fine AOD(500 nm)>1.1). Thus the conclusions and main findings of this paper are unchanged even if the fine mode AOD estimated by SDA are lower than the actual values as suggested by the Smirnov et al. (2018) simulations. However, empirical evidence of this SDA underestimate of fine mode AOD as suggested by these simulations is often lacking and not provided by Smirnov et al. (2018). For example, time series of fine mode AOD on a day with moderate to high optical depth cirrus alternating with cloudless periods often do not show a decrease in fine AOD when the cirrus is overlying the aerosol layer compared to when cirrus is not partially obscuring the sun.

The maximum AOD that can be measured by AERONET (and all sun photometers) is ~7 for overhead sun and AOD*m<7 (where m = optical airmass) for other solar zenith angles. At AOD values higher than ~7 the sun is no longer visible and significant diffuse radiation is present (direct beam signal nearly completely attenuated, see Sinyuk et al. (2012)). In Version 3 very high AOD data are retained in the longer wavelengths (675 to 1640 nm) if the Ångström Exponent is sufficiently high (>1.2 for 675–1020 nm or >1.3 for 870–1020 nm) when the solar radiation at the UV and visible wavelengths is attenuated to levels below the instrument sensitivity. However robust SDA retrievals require all wavelengths from 380 to 870 nm (5 channels) be utilized as input: therefore we do not analyze the impact of these particular extremely high AOD events in this paper. Additionally, AERONET measurements cannot detect AOD in the presence of moderate to thick clouds, including most cumulus clouds when cloud optical depth exceeds 7. As a result there is a sampling bias from AERONET measurements (and satellite retrievals also) that results in a lack of characterization of AOD in major cloud systems with moderate to high cloud optical depth. Additionally AERONET does not attempt measurements during precipitation, since a wet sensor signal keeps the instrument in parked mode (looking down) to help protect the optical lenses from water and solute contamination. However, the data that we are analyzing here of fine mode AOD from SDA retrievals of L1 data provide better characterization of AOD in the near cloud environment (as compared to cloud screened data), or in cases where few small gaps in the clouds allow for very few direct sun observations over the course of the day.

3.2 Aerosol processing by fog and/or low altitude layer cloud

In this section we examine how cloud and/or fog processing of particles may significantly modify the particle size distribution in the fine mode. In Figure 6 the South Korean Hankuk University of Foreign Studies site (Hankuk_UFS) almucantar volume size distribution retrievals from March 17, 2012 are compared with the spring season average size distribution at the Yonsei University site for the months of March through May of both 2011 and 2012. These two sites are located in the same region, ~38 km apart. On Mar 17, 2012 at the Hankuk_UFS site during the time of these almucantar retrievals the AOD at 440 nm was 1.03 and the Ångström Exponent (440–870 nm) was ~0.96. The spring season mean at the Yonsei University site was computed as the average of 42 Level 2 almucantar retrievals with a mean fine mode fraction (FMF) of AOD of 0.88 at 440 nm with AOD at 440 nm ranging from 0.6 to 0.8. The MODIS Terra image from ~4 hours after the time of the retrievals shows extensive cloud cover plus layer cloud over the Yellow Sea that may be fog. Both the smaller radius fine mode and the coarse mode size distribution of this case at Hankuk_UFS are very similar to the Yonsei climatological size distributions. The significant difference is the presence of the middle sub-micron sized mode with radius ~0.4–0.5 micron in the Hankuk_UFS retrievals. It is noted that three other sites (Yonsei University, DRAGON_NIER, and Anmyon) had almucantar retrievals on March 18, 2012 (about 8–9 hours later) that also had a sub-micron middle mode. Additionally, the Anmyon site was 126 km from Yonsei in central Seoul thus suggesting widespread presence of this middle mode particle size on this day. Both Eck et al. (2012) and Li et al. (2014) have shown this mode to be associated with cloud or fog processed aerosols and Li et al. (2014) determined that this cloud processed or residual aerosol mode was typically best fit by a size distribution with 0.44 μm median radius and width defined by geometric standard deviation of 1.49. These middle sized aerosol particles have also been measured in situ by Dall'Osto et al. (2009) associated with fog occurrence. Some chemical species of this middle mode, such as hydroxymethane sulfonate, are only formed in the aqueous phase (Munger et al., 1986; Whiteaker and Prather, 2003). This case is shown as an example of observed aerosol modification by cloud/fog in this region as part of the overall greater issue of spectral AOD observations associated with aerosol-cloud interactions (see Figure 7 below and associated text)

3.3 Observations of Near-Cloud AOD Spectra

Since the AOD spectra is the key to separating fine versus coarse modes in the SDA algorithm, we examine the spectra of a single case (and how it relates to possible middle mode aerosol mentioned above), and also the parameter $d\alpha/dln\lambda$ (α') that varies as a function of fine mode particle size (Reid et al., 1999; Eck et al., 2001), and is a key input to SDA. A single day case study at the Baengnyeong Island, South Korea site on July 13, 2012 is shown in Figure 7. There was only one observation of AOD made all day at the site due to the extensive cloud cover (see MODIS Terra image in the Figure), and the fine mode AOD retrieved from SDA was very high at 2.40 at 500 nm, with fine mode fraction of 0.97. This measured AOD spectrum suggests large fine mode particle size due to the strong spectral non-linearity of the AOD in logarithmic space with α'=1.30 (Reid et al. 1999, Eck et al. 1999, 2001). High values of spectral non-linearity can only occur when large accumulation mode particles dominate as shown from Mie calculations in Eck et al. (1999, 2001). Figure 1

of O'Neill (2005) indicates that this optical phenomena corresponds to a situation where the spectral curvature is at or near the spectral curvature of the anomalous diffraction peak of the extinction efficiency: this appears as a broad peak in α_f' (the fine mode value of α' when the fine mode fraction is large) at smaller, sub-unity values of α_f (corresponding precisely to large fine mode particles).This large fine mode particle size may be due in part to particle humidification growth in/near clouds and/or cloud processing of aerosol particles.

Mie calculations were made for a cloud processed aerosol mode as defined by Li et al. (2014), where volume median radius is 0.44 μm and geometric standard deviation is 1.49, which results in α' of 1.81 and Ångström Exponent (440–870 nm) of 0.26. The values of 1.45 and 0.01 that we assumed for the real and imaginary refractive indices are typical AERONET retrieval values for summertime pollution in Eastern China. Additional Mie calculations were performed for humidified aerosol where the assumed volume median radius was 0.25 um and the assumed geometric standard deviation was 1.49 (typical summer values for high AOD fine mode aerosol in eastern China), and where the resulting α' was 1.77 and the Ångström Exponent (440–870 nm) was 1.52. Then, AOD spectra were computed from Mie code calculations for a combined 50% cloud processed mode (0.44 μm volume radius) and 50% humidified mode (0.25 μm) resulting in α' of 1.41 and Ångström Exponent (440–870 nm) of 0.83. This case agrees closely with the measured derivatives from the AOD spectra of α' of 1.30 and Ångström Exponent (440–870 nm) of 0.80. Of course there is no way to know from available measurements if both of these assumed fine modes comprised 50% of the total AOD, and the humidified mode may have had smaller or larger fine particles than assumed here. However these Mie calculations are presented as a potential (perhaps likely) explanation of humidified plus cloud processed fine particles resulting in the observed AOD spectra.

Additionally, the satellite imagery showing extensive cloud cover along with the sparseness of AERONET measurements of AOD (also due to clouds) is consistent with the measured AOD spectra that can only be explained by large fine mode particles likely resulting from both cloud processing and aerosol humidification. This AOD spectra observation on this day at Baengnyeong was eliminated by cloud screening by both Version 2 and Version 3 cloud screening algorithms therefore the only way to detect this fine mode event with AERONET was from Level 1 data utilizing SDA. Note that of the eight other AERONET sites in South Korea on this date (July 13, 2012), three sites had no Level 1 data, while five sites had Level 1 SDA fine mode AOD(500 nm) ranging from 0.88 to 1.30, and only 1 site had three points that would pass cloud screening to Level 2 in Version 2. This sparseness of direct sun observations combined with high fine mode AOD again shows that high pollution AOD events are often associated with extensive clouds, and that these events are difficult to detect from remote sensing measurements.

The α' parameter (indicative of fine mode particle size), shows a strong increasing tendency as AOD increases, at both the XiangHe and Yonsei sites for January through May 2012 (Figure 8). This trend in α' is consistent with increasing fine mode radius as AOD increases (Eck et al, 2003, 2010). This assertion is effectively a corollary of the algorithm reported in O'Neill et al. (2005) (corrected in O'Neill et al., 2008) where it was demonstrated that the fine mode effective radius, in the presence of fixed refractive index (fixed aerosol type) was

a strong function of a ratio involving α_f' over α_f. Increases in particle radius as AOD increases may result from a combination of several physical factors: increased coagulation rates at high aerosol concentrations, humidification (sometimes in high RH cloudy environments) and also cloud processing of particles. Additionally, note that the values of α' are higher for Yonsei than for XiangHe at the same AOD levels, possibly due to further aging and processing of fine mode aerosol as it is transported from China to Korea (potentially resulting in larger fine mode particles in Korea). However much of the difference in α' is due to the frequently higher coarse mode fractions in China due to closer proximity to arid lands (dust sources), and also possibly more coarse mode fly ash associated with coal combustion and combustion of other fuels in China (Yang et al. 2009). For all observations in this time interval where AOD at 500 nm exceeded 1, the average fine mode fraction of AOD at 500 nm for the Yonsei University site was 0.92 versus 0.84 for the XiangHe site, thus on average significantly higher coarse mode was present at the site in China. These coarse mode particles may diminish from gravitational settling in transport to South Korea. Also the coarse mode particles associated with fuel combustion are not emitted as much in South Korea as compared to China, due to the number and type of sources and also emission control differences.

3.4 Comparison of MODIS Satellite Detection of Fine Mode AOD Events to AERONET

In this section we examine the ability of MODIS satellite algorithms to detect high magnitude AOD events for two selected sites in the region. The daily averages of AERONET L1 fine mode 550 nm AOD were compared to L2 and to daily spatial averages of MODIS retrievals of total AOD at the XiangHe site from Jan 1- May 18, 2012. The satellite daily data are computed by averaging retrievals over a 30 km radius for Dark Target (DT) and Deep Blue (DB), and 61 km by 61 km square for MAIAC. It is noted that AERONET has much higher sampling frequency than satellite, i.e. 15 minutes or less from solar zenith angle (SZA) of 82 degrees in the morning and to the same SZA in the evening, while MODIS has only 2 overpasses per day. However the spatial coverage of MODIS, as selected for this comparison study, is significantly greater than a single AERONET site, partially compensating for lesser temporal coverage.

The time series of SDA L1 Fine mode AOD compared to satellite retrievals of AOD by the MODIS DT algorithm shows that this algorithm screens many high AOD (> 0.8 at 550 nm) events at XiangHe in 2012. Figure 9 a.–c. shows the daily mean AOD(550 nm) time series at XiangHe for SDA L1 versus MODIS retrievals for the Collection 6 database DT, DB, and MAIAC algorithms respectively. In Table 1, the AERONET and MODIS data sets are compared for detection of high AOD events, with the threshold of AOD(550 nm)>0.8. Only one MODIS overpass retrieval having AOD(550 nm)>0.8 was required to meet the high AOD threshold for comparison purposes, while for AERONET the daily averages are required to exceed the threshold. A comparison of the AERONET SDA L1 versus L2 shows that the AERONET Version 2 cloud screening results in missing 38% of the high AOD days. Both the DB and MAIAC algorithms also had no AOD retrievals on a similar number of these days, 44% and 41% respectively. In DB, based on this analysis and others, improved smoke detection tests have recently been developed to identify thick and/or spatially-variable smoke events such as these which are screened out by the C6 algorithm version. The

upcoming MODIS C6.1 DB data set is therefore expected to suffer from less of a sampling bias in these conditions than C6. The DT algorithm retrieves AOD on only 3 days from day 1 through 80 (Jan 1 – Mar 20) in 2012. This is the main reason why the DT algorithm misses 75% of the high fine mode AOD events that are identified by SDA in Level 1. However, it is noted that for some days there is cloud cover present during the Terra and Aqua overpasses yet not cloud at some other time periods when AERONET is sampling the AOD. Additionally, since all three algorithms utilize input data from the same satellite measurements, the differences between retrievals shown here seem likely to be due in large part to differences in cloud screening.

All three MODIS AOD retrieval algorithms also added days of high AOD that are missed by AERONET L1 in SDA. For some of the highest AOD days that DB made a retrieval yet SDA L1 did not at XiangHe, the Beijing AERONET site (~60 km to the WNW of XiangHe) measured AOD>2, suggesting that clouds covered the XiangHe site for the entire day yet did not extend westward all the way to Beijing. Therefore at least some (if not most) of the added days by the MODIS retrievals were due to greater spatial sampling by the satellite, while the other possibility is potential cloud contamination of the MODIS retrievals.

Similar comparisons for the Yonsei University site in Seoul showed that all three satellite retrieval algorithms missed most days of high fine mode AOD identified by the Level 1 SDA retrievals from AERONET, missing 65%, 82% and 71% of these days for DT, DB and MAIAC respectively. However it is noted that Seoul is flanked in many directions by low altitude mountains that nonetheless extend in altitude above a fraction of the aerosol layer. Therefore spatial averages of satellite retrievals of AOD centered on the Yonsei site include lower AOD over the mountains averaged with higher AOD over the lowlands (where the Yonsei University site is located). Therefore it is expected that the spatial average satellite retrievals at Yonsei University (in Seoul) which average both samples of lower AOD over the mountains and higher AOD in the lowlands, would be biased low versus the point AERONET measurement at this lowland site.

3.5 Data Assimilation Model Identification of Major Fine Mode AOD Events

Two Data Assimilation (DA) models (NAAPS and MERRAero) both showed underestimation of Fine Mode AOD at 550 nm compared to L1 fine mode AOD from SDA, with greater underestimation for the higher AOD cases that were eliminated by L2 AERONET cloud screening (Version 2 SDA; Figure 10). Note that both the NAAPS version shown here and the MERRAaero model did not assimilate AERONET data, while the more recent MERRA-2 reanalysis does (Randles et al., 2017, Buchard et al., 2017). Data temporal collocation is important in comparison of aerosol data sets (Schutgens et al. 2016). Therefore we have compared only daytime (sunlit hours when AERONET measurements are possible) to daytime only hours of the NAAPS and MERRAero data assimilation model results. However close time matching has not been employed either with the model or satellite measurements. Therefore more frequent sampling by AERONET (15 min or 3 minute measurement interval, depending on instrument mode) from SZA of 82 degrees in the morning to 82 degrees in the evening give AERONET a much higher probability of measuring AOD in cloudy conditions. Figure 10 shows these comparisons, additionally

showing the time series of Collection 5 MODIS DT retrievals of AOD since C5 is the satellite data assimilated into the models. The lack of DT retrievals of high AOD days from day of year from 1 to ~85 clearly results in a handicap to the assimilation models. This suggests a combination of factors in the data assimilation models pertaining to underestimation of high AOD events, including possible underestimation of aerosol source functions, lack of satellite retrievals for some high AOD events, and possible insufficient humidification growth in near cloud environments. MERRAero does not include cloud processing of aerosols in the GOCART aerosol microphysical model utilized.

Rubin et al. (2017) found that assimilation of AERONET observations of AOD in addition to MODIS data into an advanced ensemble assimilation of the NAAPS model resulted in increased forecasting skill for high AOD (>1) events with improvements in temporal variability in regions such as India and east Asia. The recent MERRA-2 reanalysis also adds assimilation of AOD observations from AERONET (Randles et al., 2017) and similarly also shows improved identification of high AOD events in eastern China (Buchard et al. 2017). **In both the** Rubin et al. (2017) **NAAPS study and the** Randles et al. (2017) **MERRA-2 study the AERONET Version 2 Level 2 total AOD data were assimilated into the models. The MODIS Collection 5 AOD were also utilized or assimilated in both studies.**

3.6   Climatological Analysis of AERONET Fine Mode AOD

Comparisons utilizing AERONET multi-year cloud-screened versus non cloud-screened fine mode AOD were performed for selected sites that had at least 5 years of observations in all months. The comparisons, which included the analysis of monthly mean seasonal dynamics for this particular aerosol optical property, permitted a climatological scale analysis. AERONET data from the sites of Yonsei University (6 years data) and Anmyon (5–7 years data varying by month), both in South Korea, and also XiangHe, China (11 years data) are included in this section.

First we examine how many days of data at selected high fine mode AOD thresholds are eliminated by the L2 cloud-screening, in both Versions 2 and 3 of the AERONET data base. In Table 2 (Version 2) and Table 3 (Version 3) we show the numbers of days of fine mode AOD data in L1 and L2 and their absolute and relative differences in number of days for various thresholds of minimum AOD levels. For the XiangHe site in Version 2, Table 2 shows that 33% of the data with daily mean AOD>1 were screened at L2 while 48% were screened by L2 at AOD>2 and 64% screened for days with average AOD>3. Note that for the Xianghe site the annual average Version 2 Level 2 total AOD at 500 nm is very high at 0.76 with monthly means for all summer months (Jun, Jul, Aug) ranging from 0.95 to 1.19. However in Version 3 for the XiangHe site there were significantly fewer days eliminated by L2 cloud screening than in Version 2. For days with AOD>2 at 500 nm the V3 cloud screening eliminated 18% of the days while V2 screened 48% of the days for the same AOD threshold. Clearly the new Version 3 cloud screening and QA allows many more days of data with high levels of fine mode AOD to be analyzed. Similarly, for the Yonsei University site, for days with daily mean fine AOD>1 at 500 nm, the V2 cloud screening eliminated 38% of the days while V3 cloud screening eliminated significantly fewer days at 13%.

Comparisons of frequency histograms of days that were eliminated by L2 cloud screening (without an AOD threshold) for both Versions 2 and 3 are shown in Figure 11. These eliminated days are the ones that exist in L1 data but are screened by L2, and are designated as L0 in Arola et al. (2017). The bin width is 0.1 AOD for the daily average fine mode L0 data. For the Yonsei University site there were significantly fewer days eliminated by the V3 cloud screening and QA than the V2 screening at all AOD levels. For the XiangHe site there were significantly fewer days of data eliminated by V3 when fine AOD was greater than 1 at 500 nm. Even though the difference in number of days between V3 and V2 is relatively large for low AOD at XiangHe, there is a relatively small percentage difference (~3%, for AOD<0.5) of the ratio of eliminated days (L0) to total L1 days. The slightly greater elimination of low AOD days by V3 at this site is likely due in large part to the cirrus cloud screening check that utilizes the sky radiances in the solar aureole in V3.

In additional climatological data analysis, the L1 non cloud-screened fine mode AOD (500 nm) increases as the total number of hours of data per day of cloud-screened L2 fine mode AOD observations decreases. This occurred for both the XiangHe, China and Anmyon, South Korea sites in both winter and spring (Figure 12.). These relationships suggest that higher fine mode AOD occurs when cloud cover increases, since missing hours of data are primarily due to greater cloud cover (and/or greater temporal variability of AOD that sometimes occurs in the near vicinity of clouds (Eck et al. 2014)). Greater cloud amount may be increasing fine mode AOD through humidification (since more clouds form when RH increases), cloud processing of existing particles and/or new particle formation. Additionally it is possible that higher fine mode AOD may contribute somewhat to increasing cloud amount due to reduced or delayed precipitation (cloud lifetime effect) or other aerosol-cloud feedbacks. Another factor that needs to be considered is that the AOD spatial and temporal variance tends to increase as AOD increases thus possibly resulting in erroneous screening of high fine mode AOD as clouds in some cases. Furthermore, meteorological co-variation is likely a factor since many cloud-free days in this region occur with high atmospheric pressure systems that come from Siberia. The Siberian region has fewer aerosol sources (except when forest fires are occurring) and thus AODs tend to be smaller. Also, high-pressure systems associated with the flow from the north have subsiding air that suppresses convection and cloud formation. Another factor that needs to be considered is that for both L1 and L2 data on very high fine mode AOD days (AOD ~>2) only mid-day observations may exist due to full attenuation of the AOD signal for shorter wavelengths at large optical airmass (atmospheric path length).

The annual cycle of monthly mean fine mode AOD (500 nm) climatology using Version 2 data for both the Anmyon, South Korea site and the XiangHe, China site, show ~10–15% higher AOD for L1 non cloud-screened data as compared to L2 cloud screened data (see Figure 13a and 13b) for most months due to cloud screening of some high AOD cases and also due to elimination of high frequency AOD variability in the vicinity of cumulus clouds which also tends to have higher AOD (Eck et al. 2014). Similar large differences in climatological L1 and L2 fine mode AOD (Version 2) in Asia were also found by Arola et al. (2017), who identified that this region globally had the largest relative increases compared to all other regions. Note that for both sites the monthly mean fine mode mid-visible AOD (500 nm) increased dramatically from May to June, close to doubling at both Anmyon and

XiangHe. June peaks in AOD in East Asia have been previously noted (Eck et al., 2005; Kim et al, 2007; Koo et al., 2008) however the increase in total AOD from May to June is less of a jump than for Fine mode AOD due to increased coarse mode AOD in spring months in the region. The dramatic increases in fine mode AOD are coincident with multi-year average increases in cloud fraction and relative humidity from May to June, and also with reduction in wind speed from May to June (Figure 13c). These meteorological factors are all consistent with increases in fine mode AOD, through particle humidification and growth, cloud processing and more rapid rates of new particle formation in clouds, as well as greater buildup of pollutants during stagnation conditions. Additional factors, which may contribute to the large increases in AOD during June in the North China Plain (NCP; where the Xianghe site is located), were suggested by Qu et al. (2016). These are increased secondary organic aerosol formation due to high temperatures and higher levels of solar radiation coupled with a deeper boundary layer, plus agricultural burning emissions in summer, and southerly winds resulting in buildup of pollutants in the NCP topographical basin. One of the reasons for selecting the May through mid-June 2016 time interval for the KORUS-AQ field experiment in South Korea and surrounding waters was these projected changes in meteorology and associated impacts on atmospheric pollutants.

A comparison of the monthly mean fine mode AOD climatology for the XiangHe site between Versions 2 and 3 for matched months to the data shown in Figure 13b, is shown in Figure 13d. The Version 2 and 3 monthly means are nearly equal for April and May, however most other months show higher fine mode AOD in Version 3. The differences in monthly mean AOD range from near zero to ~0.035 from January through May however for the three summer months of June, July, August the Version 3 fine mode AOD at 500 nm is greater than Version 2 by ~0.075, 0.133 and ~0.162 respectively. The differences in AOD between the two versions is much greater in the summer months when cloud fraction is the highest, therefore suggesting (as also shown in Figure 5 and Tables 2 and 3) that Version 3 screens fewer high AOD fine mode aerosol events than Version 2. Also note that the monthly mean fine mode fractions of AOD at 500 nm are similar between Versions 2 and 3 (Figure 13e), in all months even in spring when desert dust is more prevalent (Figure 13f). However, this paper focuses primarily on the fine mode AOD and the differences that occur between Level 1 and Level 2 data and also Versions 2 and 3 of the AERONET database. The differences in coarse mode AOD for sites that are dominated by coarse mode AOD or have mixtures of fine and coarse mode will be examined in more detail in future publications.

4. Summary and Conclusions

The occurrence of events with high fine mode aerosol optical depth often associated with high cloud fraction in East Asia (Korea and upwind NE China) was examined utilizing AERONET and satellite retrievals. Analyses were focused primarily on AERONET data and included comparisons of direct sun measured AOD from the algorithms utilized in Version 2 to the newly released Version 3 data base that have significant differences in cloud screening, primarily based on temporal variance of AOD. While there are a number of cloud screening differences between V2 and V3, one of the most important differences is that temporal variance filtering is relegated to the longer, more coarse-mode-dependent, wavelengths. It is emphasized that the differences in AOD between V2 and V3 cloud-

screened data observed in this highly polluted, high AOD East Asia region may differ significantly from other regions on earth.

1. Major aerosol pollution transport events with very high Fine Mode AOD (>1.0 in mid-visible) in China/Korea/Japan were often observed to be associated with extensive cloud cover. This makes remote sensing of these events from both satellites and ground-based observations very difficult, leading to their underrepresentation in these data sets.

2. Frequently observed high levels of fine mode AOD in cloud-dominated skies suggests possible physical mechanisms such as aerosol humidification and cloud processing of aerosols resulting in very high AOD in association with extensive cloud cover in some cases. Meteorological co-variation is also possible with convergence (e.g., frontal features, Zhang and Reid 2009) resulting in higher AOD and also aerosol transport associated with mid-latitude cyclonic systems and associated frontal passages. AERONET cloud screening (Version 2) often eliminated many days with the highest AOD that were typically associated with high cloud fraction in this region in winter through summer 2012. High frequency temporal variation of AOD in the near-cloud environment, plus very few observations per day in cloud gaps, are typically the reasons that these observations are eliminated in Version 2 Level 2 AOD data.

3. The new AERONET Version 3 AOD has significantly different cloud screening algorithms than utilized in the Version 2 database. The V3 cloud screening allows more cases of fine mode pollution events that occur on predominately cloudy days to be raised to Level 2 (fully cloud screened and quality assured). Thus the V3 Level 2 AOD data allows for a more robust and physically realistic characterization of fine mode aerosol events than in V2 Level 2. However, the SDA algorithm applied to Level 1 data (no cloud screening) provides an even more comprehensive assessment of fine mode AOD than Level 2 in both V2 and V3, provided that the L1 data have final calibrations and specific additional quality control checks.

4. Additionally, comparison to AERONET L1 SDA daily average fine mode AOD data shows that MODIS (Dark Target, Deep Blue and MAIAC algorithms) remote sensing of AOD often did not retrieve and/or identify some of the highest fine mode AOD events in this region/season in 2012 (for sites in both Xianghe, China and Seoul, South Korea). For the Yonsei University site in Seoul all three MODIS algorithms missed the majority of high AOD days likely due in part to the complexity of the terrain with highly urbanized valleys surrounded by densely forested mountains. This is illustrative of difficulties in aerosol remote sensing and the fact that sampling biases in these data sets can be systematic (i.e. will not be cancelled out by temporal averaging). Also NAAPS & MERRA modeling of AOD (assimilating MODIS DT C5 AOD data) compared to L1 SDA fine mode AOD showed that both assimilation models significantly underestimated the magnitude of fine AOD especially for the highest fine mode AOD events that were often associated with significant cloudiness.

5. The relatively frequent satellite retrieval screening-out of some high fine mode AOD events in the proximity of clouds in East Asia suggests that the relationships between cloud cover and AOD as determined from satellite data may not be fully characterized in this East Asia region.

More detailed investigation of differences in AERONET Version 2 and 3 AOD data sets, including fine and coarse mode AOD, will be the topic of future studies.

Acknowledgements

References

Albrecht BA (1989), Aerosols, cloud microphysics, and fractional cloudiness, Science, 245 (4923), 1227–1230. [PubMed: 17747885]

Arola A, Eck TF, Kokkola H, Pitkänen MRA, and Romakkaniemi S (2017), Assessment of cloud-related fine-mode AOD enhancements based on AERONET SDA product, Atmos. Chem. Phys, 17, 5991–6001, doi:10.5194/acp-17-5991-2017.

Buchard V, et al. (2015), Using the OMI aerosol index and absorption aerosol optical depth to evaluate the NASA MERRA Aerosol Reanalysis, Atmos. Chem. Phys, 15, 5743–5760, doi:10.5194/acp-15-5743-2015

Buchard V, et al. (2016), Evaluation of the surface PM 2.5 in version 1 of the NASA MERRA Aerosol Reanalysis over the United States. Atmos. Environ, 125, 100–111, doi:10.1016/j.atmosenv.2015.11.004

Buchard V, Randles CA, da Silva AM, Darmenov A, Colarco PR, Govindaraju R, Ferrare R, Hair J, Beyersdorf AJ, Ziemba LD, and Yu H (2017), The MERRA-2 Aerosol Reanalysis, 1980 Onward. Part II: Evaluation and Case Studies, Journal of Climate, Vol. 30, No. 17.

Chew BN, Campbell JR, Reid JS, Giles DM, Welton EJ, Salinas SV, and Liew SC (2011), Tropical cirrus cloud contamination in sun photometer data, Atmospheric Environment, 45 (2011), 6724–6731, doi:10.1016/j.atmosenv.2011.08.017

Chin M et al. (2002), Tropospheric aerosol optical thickness from the GOCART model and comparisons with satellite and Sun photometer measurements, J. Atm. Sci, 59, 3, 461–483.

Clarke AD, Howell S, Quinn PK, Bates TS, Ogren JA, Andrews E, Jefferson A, Massling A, Mayol Bracero O, Maring H, Savoie D, and Cass G (2002), INDOEX aerosol: A comparison and summary of chemical, microphysical, and optical properties observed from land, ship, and aircraft, J. Geophys. Res, 107(D19), 8033, doi:10.1029/2001JD000572,.

Colarco Peter; da Silva Arlindo; Chin Mian, and Diehl T (2010), Online simulations of global aerosol distributions in the NASA GEOS-4 model and comparisons to satellite and ground-based aerosol optical depth, J. Geophys. Res, Vol. 115, D14207,.

Dall'Osto M, Harrison RM, Coe H, and Williams P (2009), Real-time secondary aerosol formation during a fog event in London, Atmos. Chem. Phys, 9, 2459–2469.

Dubovik O, and King MD (2000), A flexible inversion algorithm for the retrieval of aerosol optical properties from Sun and sky radiance measurements, J. Geophys. Res, 105, 20,673–20,696,.

Dubovik O, Smirnov A, Holben BN, King MD, Kaufman YJ, Eck TF, and Slutsker I (2000), Accuracy assessments of aerosol optical properties retrieved from AERONET Sun and sky-radiance measurements, J. Geophys. Res, 105, 9791– 9806,.

Dubovik O, Sinyuk A, Lapyonok T, Holben BN, Mishchenko M, Yang P, Eck TF, Volten H, Muñoz O, Veihelmann B, van der Zande WJ, Leon J-F, Sorokin M, and Slutsker I (2006), The application of

spheroid models to account for aerosol particle nonsphericity in remote sensing of desert dust, J. Geophys. Res, 111, D11208, doi:10.1029/2005JD006619,.

Eck TF, Holben BN, Reid JS, Dubovik O, Smirnov A, O'Neill NT, Slutsker I, and Kinne S (1999), Wavelength dependence of the optical depth of biomass burning, urban, and desert dust aerosols, J. Geophys. Res, 104(D24), 31,333–31,349,.

Eck TF, Holben BN, Ward DE, Dubovik O, Reid JS, Smirnov A, Mukelabai MM, Hsu NC, O'Neill NT, and Slutsker I (2001), Characterization of the optical properties of biomass burning aerosols in Zambia during the 1997 ZIBBEE Field Campaign, J. Geophys. Res, 106, 3425–3448.

Eck TF, Holben BN, Reid JS, O'Neill NT, Schafer JS, Dubovik O, Smirnov A, Yamasoe MA, and Artaxo P (2003), High aerosol optical depth biomass burning events: A comparison of optical properties for different source regions, Geophys. Res. Lett, 30, 2035, doi:10.1029/2003GL017861, 20.

Eck TF, et al. (2005), Columnar aerosol optical properties at AERONET sites in central eastern Asia and aerosol transport to the tropical mid-Pacific, J. Geophys. Res, 110, D06202, doi:10.1029/2004JD005274.

Eck TF, Holben BN, Reid JS, Sinyuk A, Dubovik O, Smirnov A, Giles D, O'Neill NT, Tsay S-C, Ji Q, Mandoos AA, Khan MR, Reid EA, Schafer JS, Sorokine M, Newcomb W, and Slutsker I (2008), Spatial and temporal variability of column-integrated aerosol optical properties in the southern Arabian Gulf and United Arab Emirates in summer, J. Geophys. Res, 113, D01204, doi:10.1029/2007JD008944,.

Eck TF, Holben BN, Sinyuk A, Pinker RT, Goloub P, Chen H, Chatenet B, Li Z, Singh RP, Tripathi SN, Reid JS, Giles DM, Dubovik O, O'Neill NT, Smirnov A, Wang P, and Xia X (2010), Climatological aspects of the optical properties of fine/coarse mode aerosol mixtures, J. Geophys. Res,115, D19205, doi:10.1029/2010JD014002,.

Eck TF, Holben BN, Reid JS, Giles DM, Rivas MA, Singh RP, Tripathi SN, Bruegge CJ, Platnick S, Arnold GT, Krotkov NA, Carn SA, Sinyuk A, Dubovik O, Arola A, Schafer JS, Artaxo P, Smirnov A, Chen H, and Goloub P (2012), Fog- and cloud-induced aerosol modification observed by the Aerosol Robotic Network (AERONET), J. Geophys. Res, 117, D07206, doi:10.1029/2011JD016839,.

Eck TF, Holben BN, Reid JS, Arola A, Ferrare RA, Hostetler CA, Crumeyrolle SN, Berkoff TA, Welton EJ, Lolli S, Lyapustin A, Wang Y, Schafer JS, Giles DM, Anderson BE, Thornhill KL, Minnis P, Pickering KE, Loughner CP, Smirnov A, and Sinyuk A (2014), Observations of rapid aerosol optical depth enhancements in the vicinity of polluted cumulus clouds, Atmos. Chem. Phys, 14, 11633–11656, doi:10.5194/acp-14-11633-2014,.

Ervens B, Turpin BJ, and Weber RJ (2011), Secondary organic aerosol formation in cloud droplets and aqueous particles (aqSOA): a review of laboratory, field and model studies, Atmos. Chem. Phys, 11, 11069–11102, doi:10.5194/acp-11-11069-2011,.

Ginoux Paul, Chin M, Tegen I, Prospero JM, Holben B, Dubovik O, and Shian-Jiann Lin (2001), Sources and distributions of dust aerosols simulated with the GOCART model. J. Geophys. Res., 106(D17), 20255–20273,.

Grandey BS, Stier P, and Wagner TM (2013a), Investigating relationships between aerosol optical depth and cloud fraction using satellite, aerosol reanalysis and general circulation model data, Atmos. Chem. Phys, 13, 3177–3184, doi:10.5194/acp-13-3177-2013,.

Grandey BS, Stier P, Grainger RG, and Wagner TM (2013b), The contribution of the strength and structure of extratropical cyclones to observed cloud–aerosol relationships, Atmos. Chem. Phys, 13, 10689–10701, doi:10.5194/acp-13-10689-2013,.

Gryspeerdt E, Quaas J, and Bellouin N (2016), Constraining the aerosol influence on cloud fraction, J. Geophys. Res, 121, 3566–3583, doi:10.1002/2015JD023744.

Hansen ADA, Benner WH, Novakov T (1991), Sulfur-dioxide oxidation in laboratory clouds, Atmospheric Environment Part A-General Topics, 25, 11, 2521–2530, doi:10.1016/0960-1686(91)90168-7,.

Hayden KL, Macdonald AM, Gong W, Toom-Sauntry D, Anlauf KG, Leithead A, Li S-M, Leaitch WR, and Noone K (2008), Cloud processing of nitrate, J. Geophys. Res, 113, D18201, doi:10.1029/2007JD009732,.

Hogan TF, Liu M, Ridout JS, Peng MS, Whitcomb TR, Ruston BC, Reynolds CA, Eckermann SD, Moskaitis JR, Baker NL, McCormack JP, Viner KC, McLay JG, Flatau MK, Xu L, Chen C, and Chang SW, (2014), The Navy Global Environmental Model. Oceanography, Special Issue on Navy Operational Models, 27, No. 3..

Holben BN, Eck TF, Slutsker I, Tanre D, Buis JP, Setzer A, Vermote E, Reagan J Kaufman A, Nakajima Y, Lavenu TF, Jankowiak I, and Smirnov A (1998), AERONET-A federated instrument network and data archive for aerosol characterization, Remote Sens. Environ, 66, 1–16,.

Holben BN, Eck TF, Slutsker I, Smirnov A, Sinyuk A, Schafer J, Giles D, and Dubovik O (2006), AERONET's version 2.0 quality assurance criteria, Remote Sensing of Atmosphere and Clouds, Proc. SPIE Int. Soc. Opt. Eng, 6408, 64080Q, doi:10.1117/12.706524,.

Holben BN, Kim J, Sano I, Mukai S, Eck TF, Giles DM, Schafer JS, Sinyuk A, Slutsker I, Smirnov A, Sorokin M, Anderson BE, Che H, Choi M, Crawford JE, Ferrare RA, Garay MJ, Jeong U, Kim M, Kim W, Knox N, Li Z, Lim HS, Liu Y, Maring H, Nakata M, Pickering KE, Piketh S, Redemenn J, Reid JS, Salinas S, Seo S, Tan F, Tripathi SN, Toon OB, and Xiao Q (2017), An overview of meso-scale aerosol processes, comparison and validation studies from DRAGON networks, Atmos. Chem. Phys. Discuss, 10.5194/acp-2016-1182, in review,.

Hoppel WA, Frick GM, and Larson RE (1986), Effects on non-precipitating clouds on the aerosol size distribution in the marine boundary layer, Geophys. Res. Lett, 13, 125–128.

Hsu NC, Tsay SC, King MD, and Herman JR (2004), Aerosol properties over bright-reflecting source regions, IEEE Trans. Geosci. Remote Sens, 42, 557–569.

Hsu NC, Tsay SC, King MD, and Herman JR (2006), Deep blue retrievals of Asian aerosol properties during ACE-Asia, IEEE Trans. Geosci. Remote Sens, 44, 3180–3195.

Hsu NC, Jeong M-J, Bettenhausen C, Sayer AM, Hansell R, Seftor CS, Huang J, and Tsay S-C (2013), Enhanced Deep Blue aerosol retrieval algorithm: The second generation, J. Geophys. Res, 118, 9296–9315, doi:10.1002/jgrd.50712.

Hyer EJ, Reid JS, and Zhang J, (2011), An over-land aerosol optical depth data set for data assimilation by filtering, correction, and aggregation of MODIS Collection 5 optical depth retrievals, Atmos. Meas. Tech, 4, 379–408.

IPCC (2013): Climate Change 2013: The Physical Science Basis Contribution of Working Group I to the Fifth Assessment Report of the Intergovernmental Panel on Climate Change [Stocker TF, Qin D, Plattner G-K, Tignor M, Allen SK, Boschung J, Nauels A, Xia Y, Bex V and Midgley PM (eds.)]. Cambridge University Press, Cambridge, United Kingdom and New York, NY, USA, 1535 pp, doi:10.1017/CBO9781107415324.

Jeong M-J and Li Z (2010), Separating real and apparent effects of cloud, humidity, and dynamics on aerosol optical thickness near cloud edges, J. Geophys. Res, 115, D00K32, doi:10.1029/2009JD013547,.

Johnson BT and Osborne SR (2011), Physical and optical properties of mineral dust aerosol measured by aircraft during the GERBILS campaign. Q. J. R. Meteorol. Soc. DOI:10.1002/qj.777.

Joyce RJ, Janowiak JE, Arkin PA, Xie P, (2004), CMORPH: a method that produces global precipitation estimates from passive microwave and infrared data at high spatial and temporal resolution. J. Hydromet, 5, 487–503,.

Kaku KC, Reid JS, O'Neill NT, Quinn PK, Coffman DJ, and Eck TF: Verification and application of the extended spectral deconvolution algorithm (SDA+) methodology to estimate aerosol fine and coarse mode extinction coefficients in the marine boundary layer, Atmos. Meas. Tech, 7, 3399–3412, 10.5194/amt-7-3399-2014, 2014.

Kaufman YJ, Remer LA; Tanre D; Rong-Rong Li; Kleidman R; Mattoo S; Levy RC; Eck TF; Holben BN; Ichoku C; Martins JV; Koren I (2005), A critical examination of the residual cloud contamination and diurnal sampling effects on MODIS estimates of aerosol over ocean, IEEE Transactions on Geoscience and Remote Sensing, 43, 12, 2886–2897, DOI: 10.1109/TGRS.2005.858430

Kim SW, Yoon S-C, Kim J, Kim S-Y (2007), Seasonal and monthly variations of columnar aerosol optical properties over East Asia determined from multi-year MODIS, LIDAR, and AERONET sun/sky radiometer measurements. Atmos. Environ. 41, 1634–1651.

Koo J-H (2008). Optical Properties of Aerosol in a Megacity, Seoul From Ground-based and Satellite Measurements, (M.S. thesis) Dept. of Atmospheric Sciences, The Yonsei University.

Lee HJ and Son Y-S (2016), Spatial Variability of AERONET Aerosol Optical Properties and Satellite Data in South Korea during NASA DRAGON-Asia Campaign, Environmental Science & Technology, 50 (7), 3954–3964, DOI: 10.1021/acs.est.5b04831 [PubMed: 26953969]

Levy RC, Remer LA, Mattoo S, Vermote EF, and Kaufman YJ (2007), Second-generation operational algorithm: Retrieval of aerosol properties over land from inversion of Moderate Resolution Imaging Spectroradiometer spectral reflectance, J. Geophys. Res, 112, D13211, doi:10.1029/2006JD007811.

Levy RC, Mattoo S, Munchak LA, Remer LA, Sayer AM, Patadia F, and Hsu NC (2013), The Collection 6 MODIS aerosol products over land and ocean, Atmos. Meas. Tech, 6, 2989–3034, doi:10.5194/amt-6-2989-2013.

Levy RC, Munchak LA, Mattoo S, Patadia F, Remer LA, and Holz RE (2015), Towards a long-term global aerosol optical depth record: applying a consistent aerosol retrieval algorithm to MODIS and VIIRS-observed reflectance, Atmos. Meas. Tech, 8, 4083–4110, doi:10.5194/amt-8-4083-2015.

Li Z, Eck T, Zhang Y, Zhang Y, Li D, Li L, Xu H, Hou W, Lv Y, Goloub P, and Gu X (2014), Observations of residual submicron fine aerosol particles related to cloud and fog processing during a major pollution event in Beijing, Atmos. Environ, Vol. 86, 187–192, doi:10.1016/j.atmosenv.2013.12.044.

Lyapustin A, Martonchik J, Wang Y, Laszlo I, Korkin S (2011a), Multi-Angle Implementation of Atmospheric Correction (MAIAC): 1. Radiative Transfer Basis and Look-Up Tables, J. Geophys. Res, 116, D03210, doi:10.1029/2010JD014985.

Lyapustin A, Wang Y, Laszlo I, Kahn R, Korkin S, Remer L, Levy R, and Reid JS (2011b), Multi-Angle Implementation of Atmospheric Correction (MAIAC): 2. Aerosol Algorithm, J. Geophys. Res, 116, D03211, doi:10.1029/2010JD014986.

Lyapustin A, Wang Y, Laszlo I, Hilker T, Hall F, Sellers P, Tucker J, Korkin S (2012a), Multi-Angle Implementation of Atmospheric Correction for MODIS (MAIAC). 3: Atmospheric Correction. Rem. Sens. Environ., 10.1016/j.rse.2012.09.002.

Lyapustin A, Korkin S, Wang Y, Quayle B, and Laszlo I (2012b), Discrimination of biomass burning smoke and clouds in MAIAC algorithm, Atmos. Chem. Phys, 12, 9679–9686, doi:10.5194/acp-12-9679-2012.

Lyapustin A, Wang Y, Xiong X, Meister G, Platnick S, Levy R, Franz B, Korkin S, Hilker T, Tucker J, Hall F, Sellers P, Wu A, and Angal A (2014a), Scientific impact of MODIS C5 calibration degradation and C6+ improvements, Atmos. Meas. Tech, 7, 4353–4365, doi:10.5194/amt-7-4353-2014.

Lyapustin A, Wang Y, Xiong X, Meister G, Platnick S, Levy R, Franz B, Korkin S, Hilker T, Tucker J, Hall F, Sellers P, Wu A, Angal A (2014b), Science Impact of MODIS C5 Calibration Degradation and C6+ Improvements, Atmos. Meas. Tech, 7, 4353–4365, doi:10.5194/amt-7-4353-2014.

Lynch P, Reid JS, Westphal DL, Zhang J, Hogan TF, Hyer EJ, Curtis CA, Hegg DA, Shi Y, Campbell JR, Rubin JI, Sessions WR, Turk FJ, and Walker AL (2016), An 11-year global gridded aerosol optical thickness reanalysis (v1.0) for atmospheric and climate sciences, Geosci. Model Dev., 9, 1489–1522, 10.5194/gmd-9-1489-2016,.

Marshak A, Wen G, Coakley JA Jr., Remer LA, Loeb NG, Cahalan RF (2008), A simple model for the cloud adjacency effect and the apparent bluing of aerosols near clouds. J. Geophys. Res., 113, D14S17,.

Martins VS, Lyapustin A, de Carvalho LAS, Barbosa CCF, and Novo EMLM (2017), Validation of high-resolution MAIAC aerosol product over South America, J. Geophys. Res. Atmos., 122, doi:10.1002/2016JD026301.

Munger JW, Tiller C, Hoffmann MR (1986), Identification of Hydroxymethanesulfonate in Fog Water, Science, 231, 247–249. [PubMed: 17769644]

Noone KJ, Ogren JA, Hallberg A, Heintzenberg J, Ström J, Hansson H-C, Svenningsson B, Wiedensohler A, Fuzzi S, Facchini MC, Arends BG And Berner A (1992), Changes in aerosol

size- and phase distributions due to physical and chemical processes in fog. Tellus B, 44: 489–504. doi: 10.1034/j.1600-0889.1992.t01-4-00004.x

O'Neill NT, Eck TF, Holben BN, Smirnov A, Dubovik O, and Royer A (2001), Bimodal size distribution influences on the variation of Ångström derivatives in spectral and optical depth space, J. Geophys. Res., 106, 9787–9806,.

O'Neill NT, Eck TF, Smirnov A, Holben BN, and Thulasiraman S (2003), Spectral discrimination of coarse and fine mode optical deph, J. Geophys. Res., 108(D17), 4559, doi:10.1029/2002JD00297,.

O'Neill NT, Thulasiraman S, Eck TF, and Reid JS (2005), Robust optical features of fine mode size distributions: Application to the Quebec smoke event of 2002. Journal of Geophysical Research, 110(D11).

Pope CA III (2000). Epidemiology of fine particulate air pollution and human health: biologic mechanisms and who's at risk? Environ. Health Perspect. 108: 713–723.

Pueschel RF, Russell PB, Allen DA, Ferry GV, Snetsinger KG, Livingston JM, and Verma S (1994), Physical and optical properties of the Pinatubo volcanic aerosol: Aircraft observations with impactors and a Sun-tracking photometer, J. Geophys. Res., 99(D6), 12,915–12,922.

Qu W, Wang J, Zhang X, Sheng L, Wang W (2016), Opposite seasonality of the aerosol optical depth and the surface particulate matter concentration over the north China Plain, Atmos. Environ., Volume: 127, 90–99, DOI: 10.1016/j.atmosenv.2015.11.061.

Quaas J, Stevens B, Stier P, and Lohmann U (2010), Interpreting the cloud cover – aerosol optical depth relationship found in satellite data using a general circulation model, Atmos. Chem. Phys., 10, 6129–6135, doi:10.5194/acp-10-6129-2010,.

Randles CA, da Silva AM, Buchard V, Colarco PR, Darmenov A, Govindaraju R, Smirnov A, Holben B, Ferrare R, Hair J, Shinozuka Y, and Flynn CJ (2017), The MERRA-2 Aerosol Reanalysis, 1980 Onward. Part I: System Description and Data Assimilation Evaluation, Journal of Climate, Vol. 30, No. 17

Reid JS, Eck TF, Christopher SA, Hobbs PV, and Holben BN (1999), Use of the Ångström exponent to estimate the variability of optical and physical properties of aging smoke particles in Brazil, J. Geophys. Res., 104, 27,473–27,489,.

Reid JS, Koppmann R, Eck T, and Eleuterio D (2005), A review of biomass burning emissions part II: Intensive physical properties of biomass burning particles, Atmos. Chem. Phys, 5, 799–825, SRef-ID: 1680–7324/acp/2005-5-799.

Reid JS, Brooks B, Crahan KK, Hegg DA, Eck TF, O'Neill N, de Leeuw G, Reid EA, and Anderson KD (2006), Reconciliation of coarse mode sea-salt aerosol particle size measurements and parameterizations at a subtropical ocean receptor site, J. Geophys. Res, 111, D02202, doi:10.1029/2005JD006200,.

Reid JS., Rei EA, Walker A, Piketh S, Cliff S, Al Mandoos A, Tsay S-C, and Eck TF (2008), Dynamics of southwest Asian dust particle size characteristics with implications for global dust research, J. Geophys. Res., 113, D14212, doi:10.1029/2007JD009752,.

Reid JS; Hyer EJ, Prins EM, Westphal DL, Zhang J, Wang J, Christopher SA, Curtis CA, Schmidt CC, Eleuterio DP, Richardson KA, Hoffman JP (2009), Global Monitoring and Forecasting of Biomass-Burning Smoke: Description of and Lessons From the Fire Locating and Modeling of Burning Emissions (FLAMBE) Program, IEEE Journal of Selected Topics in Applied Earth Observations And Remote Sensing, 2 (3), 144–162,.

Reid JS et al. (2013), Observing and understanding the Southeast Asian aerosol system by remote sensing: An initial review and analysis for the Seven Southeast Asian Studies (7SEAS) program, Atmos. Res., 122, pp. 403–468,.

Rieneker MM et al. (2011), MERRA: NASA's Modern-Era Retrospective Analysis for Research and Applications, J. Climate, Vol. 24,Issue: 14, Pages: 3624–3648,.

Remer LA, Mattoo S, Levy RC, and Munchak LA (2013) MODIS 3 km aerosol product: algorithm and global perspective, Atmos. Meas. Tech, 6, 1829–1844, doi:10.5194/amt-6-1829-2013.

Rubin JI, Reid JS, Hansen J JA. Anderson L, Holben BN, Xian P, Westphal DL, and Zhang J (2017), Assimilation of AERONET and MODIS AOT observations using variational and ensemble data assimilation methods and its impact on aerosol forecasting skill, J. Geophys. Res., 122, 4967–4992, doi:10.1002/2016JD026067.

Saide PE, Carmichael GR, Liu Z, Schwartz CS, Lin HC, da Silva AM, Hyer E (2013), Aerosol optical depth assimilation for a size-resolved sectional model: impacts of observationally constrained, multi-wavelength and fine mode retrievals on regional scale analyses and forecasts, Atmos. Chem. Phys., Volume: 13, Issue: 20, 10425–10444.

Sano I, Mukai S, Nakata M, and Holben BN (2016), Regional and local variations in atmospheric aerosols using ground-based sun photometry during Distributed Regional Aerosol Gridded Observation Networks (DRAGON) in 2012, Atmos. Chem. Phys., 16, 14795–14803, doi:10.5194/acp-16-14795-2016.

Sayer AM, Hsu NC, Bettenhausen C, and Jeong M-J (2013), Validation and uncertainty estimates for MODIS Collection 6 "Deep Blue" aerosol data, J. Geophys. Res., 118, 7864–7872, doi:10.1002/jgrd.50600.

Sayer AM, Munchak LA, Hsu NC, Levy RC, Bettenhausen C, and Jeong M-J (2014), MODIS Collection 6 aerosol products: Comparison between Aqua's e-Deep Blue, Dark Target, and "merged" data sets, and usage recommendations, J. Geophys. Res., 119, 13,965–13,989, doi:10.1002/2014JD022453.

Sayer AM, Hsu NC, and Bettenhausen C (2015a), Implications of MODIS bow-tie distortion on aerosol optical depth retrievals, and techniques for mitigation, Atmos. Meas. Tech, 8, 5277–5288, doi:10.5194/amt-8-5277-2015.

Sayer AM, Hsu NC, Bettenhausen C, Jeong M-J, and Meister G (2015b), Effect of MODIS Terra radiometric calibration improvements on Collection 6 Deep Blue aerosol products: Validation and Terra/Aqua consistency, J. Geophys. Res, 120, 12,157–12,174, doi:10.1002/2015JD023878.

Schmid B, Michalsky J, Halthore R, Beauharnois M, Harrison L, Livingston J, Russell P, Holben B, Eck T, and Smirnov A (1999), Comparison of aerosol optical depth from four solar radiometers during the fall 1997 ARM intensive observation period, Geophys. Res. Lett, 26, 2725–2728.

Schutgens NAJ, Partridge DG, and Stier P (2016), The importance of temporal collocation for the evaluation of aerosol models with observations, Atmos. Chem. Phys, 16, 1065–1079, doi:10.5194/acp-16-1065-2016.

Shi Y, Zhang J, Reid JS, Liu B, and Hyer EJ (2014), Critical evaluation of cloud contamination in the MISR aerosol products using MODIS cloud mask products, Atmos. Meas. Tech, 7, 1791–1801,.

Shi Y (2015), Critical evaluations of MODIS and MISR satellite aerosol products for aerosol modelling applications, PhD dissertation, University of North Dakota.

Sinyuk A, Holben BN, Smirnov A, mEck TF, Slutsker I, Schafer JS, Giles DM, and Sorokin M (2012), Assessment of error in aerosol optical depth measured by AERONET due to aerosol forward scattering, Geophys. Res. Lett., 39, L23806, doi:10.1029/2012GL053894.

Smirnov A, Holben BN, Eck TF, Dubovik O, and Slutsker I (2000), Cloud screening and quality control algorithms for the AERONET data base, Remote Sens. Environ., 73, 337–349.

Smirnov A, Holben BN, Dubovik O, Frouin R, Eck TF, and Slutsker I (2003), Maritime component in aerosol optical models derived from Aerosol Robotic Network data, J. Geophys. Res., 108(D1), 4033, doi:10.1029/2002JD002701,.

Smirnov A, Zhuravleva TB, Segal-Rosenheimer M and Holben BN (2018), Limitations of AERONET SDA product in presence of cirrus clouds, Journal of Quantitative Spectroscopy and Radiative Transfer, Volume 206, Pages 338–341.

Su W, Schuster GL, Loeb NG, Rogers RR, Ferrare RA, Hostetler CA, Hair JW, and Obland MD (2008), Aerosol and cloud interaction observed from high spectral resolution lidar data, J. Geophys. Res, 113, D24202, doi:10.1029/2008JD010588.

Superczynski S, Kondragunta S, Lyapustin A (2017), Evaluiation of the Multi-Angle Implementation of Atmospheric Correction (MAIAC) Aerosol Algorithm through Inter-comparison with VIIRS Aerosol Products and AERONET, J. Geophys. Res,122,3005–3022, doi:10.1002/2016JD025720.

Tackett JL and Di Girolamo L (2009), Enhanced aerosol backscatter adjacent to tropical trade wind clouds revealed by satellite-based lidar, Geophys. Res. Lett, 36, L14804, doi:10.1029/2009GL039264.

Toller G, Xiaoxiong X, Sun J, Wenny BN, Geng X, Kuyper J, Angal A, Chen H, Madhavan S, and Wu A (2013), Terra and Aqua Moderate-Resolution Imaging Spectroradiometer collection 6 level 1b algorithm, J. Appl. Remote Sens, 7(1), 073557, doi:10.1117/1.JRS.7.073557.

Várnai T, and Marshak A (2009), MODIS observations of enhanced clear sky reflectance near clouds, Geophys. Res. Lett, 36, L06807, doi:10.1029/2008GL037089.

Várnai T and Marshak A (2011), Global CALIPSO Observations of Aerosol Changes Near Clouds, IEEE Geosci. Remote Sens. Lett, 8(1), 19–23.

Wang Y, Wang M, Zhang R, Ghan SJ, Lin Y, Hu J, Pan B, Levy M, Jiang JH, and Molina MJ (2014), Assessing the effects of anthropogenic aerosols on Pacific storm track using a multiscale global climate model, PNAS, 111 (19) 6894–6899, doi:10.1073/pnas.1403364111 [PubMed: 24733923]

Westphal DL, Toon OB, Carlson TN (1987), A two-dimensional numerical investigation of the dynamics and microphysics of Saharan dust storms, Journal of Geophysical Research, 92, D3, 3027–3049, doi: 10.1029/JD092iD03p03027,.

Whiteaker JR and Prather KA (2003), Hydroxymethanesulfonate as a tracer for fog processing of individual aerosol particles, Atmos. Environ, 37, 1033–1043.

Witek ML, Flatau PJ, Quinn PK, and Westphal DL (2007), Global sea-salt modeling: Results and validation against multicampaign shipboard measurements, J. Geophys. Res, 112.

Xian P, Reid JS, Turk JF, Hyer EJ and Westphal DL (2009), Impact of models versus satellite measured tropical precipitation on regional smoke optical thickness in an aerosol transport model, Geophys. Res. Lett, 36, L16805, doi:10.1029/2009GL038823,.

Yang M, Howell SG, Zhuang J, and Huebert BJ (2009), Attribution of aerosol light absorption to black carbon, brown carbon, and dust in China—Interpretations of atmospheric measurements during EASTAIRE, Atmos. Chem. Phys, 9, 2035–2050.

Yang W, Marshak A, Varnai T, Liu Z (2012) Effect of CALIPSO cloud-aerosol discrimination (CAD) confidence levels on observations of aerosol properties near clouds, Atmospheric Research, 116, 134–141, doi: 10.1016/j.atmosres.2012.03.013.

Yi B, Rapp AD, Yang P, Baum BA, and King MD (2017), A comparison of Aqua MODIS ice and liquid water cloud physical and optical properties between collection 6 and collection 5.1: Pixel-to-pixel comparisons, J. Geophys. Res, 122, 4528–4549, doi:10.1002/2016JD025586.

Zhang J, Reid JS, and Holben BN (2005), An analysis of potential cloud artifacts in MODIS over ocean aerosol optical thickness products, Geophys. Res. Lett, 32, L15803, doi:10.1029/2005GL023254.

Zhang J and Reid JS (2006), MODIS Aerosol Product Analysis for Data Assimilation: Assessment of Level 2 Aerosol Optical Thickness Retrievals, J. Geophys. Res, 111, 22207, doi:10.1029/2005JD006898,.

Zhang J, Reid JS, Westphal DL, Baker NL, and Hyer EJ (2008), A system for operational aerosol optical depth data assimilation over global oceans, J. Geophys. Res, 113, D10208, doi:10.1029/2007JD009065.

Zhang J, and Reid JS (2009), An analysis of clear sky and contextual biases using an operational over ocean MODIS aerosol product, Geophys. Res. Lett, 36, L15824, doi:10.1029/2009GL038723

Zhang R, Li G, Fan J, Wu DL, and Molina MJ (2007), Intensification of Pacific storm track linked to Asian pollution, PNAS, 104 (13), 5295–5299, doi:10.1073/pnas.0700618104 [PubMed: 17374719]

Key Points

- Major pollution events with high fine mode AOD in Eastern China and South Korea are often associated with significant cloud cover

- New AERONET Version 3 cloud screening allows more AOD observations in the near cloud environment to be raised to Level 2

- MODIS satellite retrieval algorithms of AOD (collections 5 and 6.0) often screened out a significant number of high fine mode AOD days
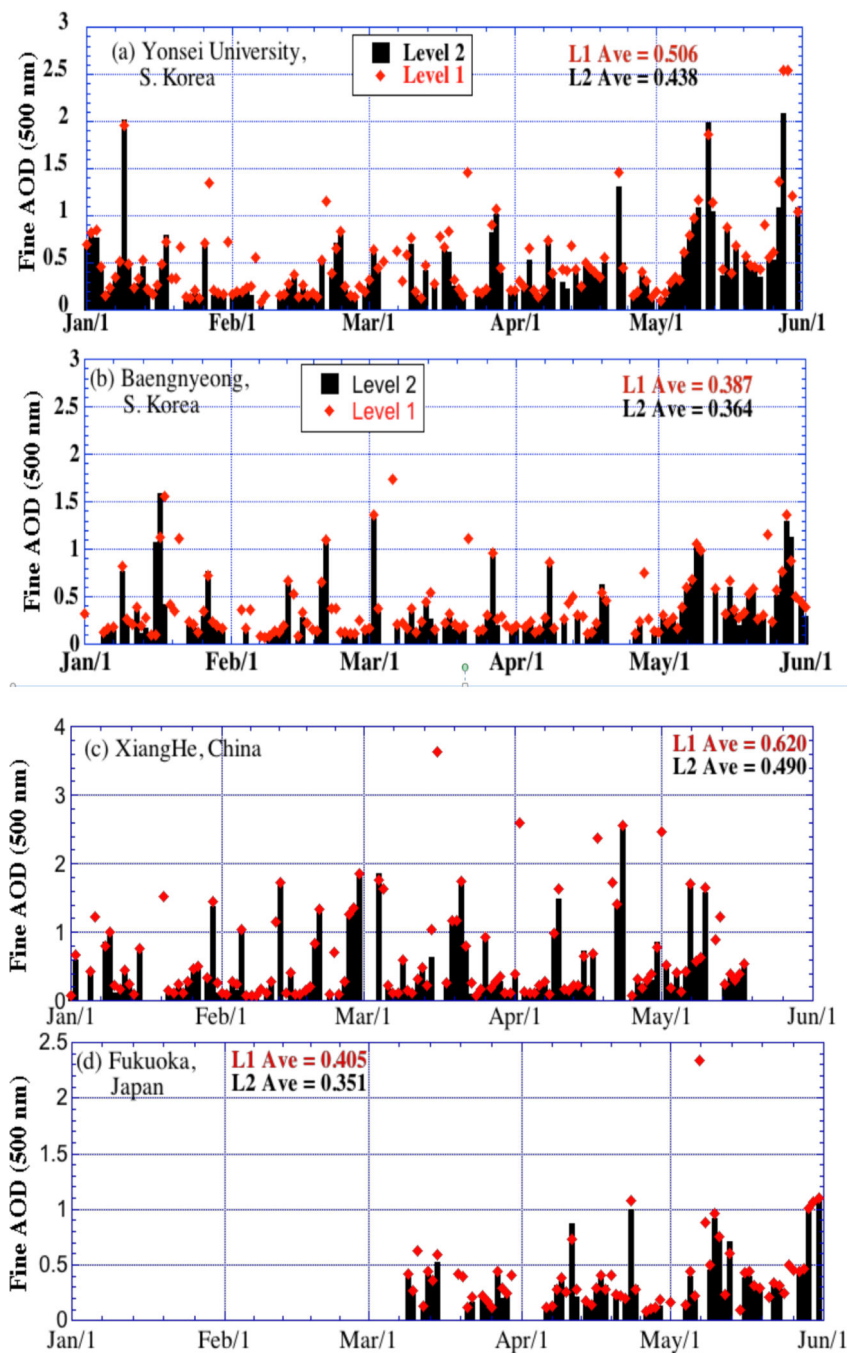
Figure 1.
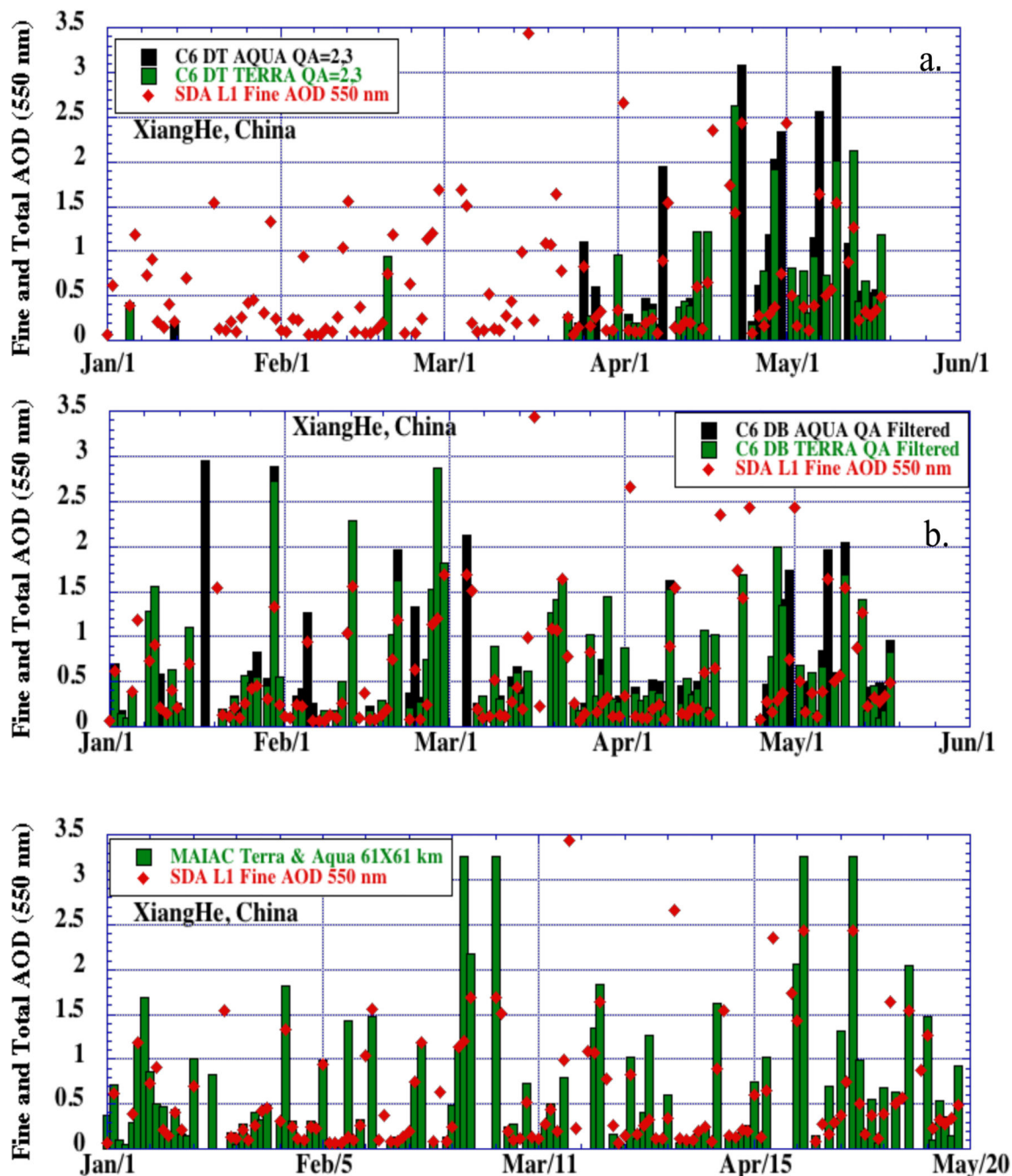Time series of daily averages of fine mode AOD at 500 nm (Version 2, V2) retrieved from
SDA from January 1 – June 1, 2012 for AERONET sites at (a) Yonsei University, S. Korea
(b) Baengnyeong, S. Korea (c) XiangHe, China and d) Fukuoaka, Japan. Note that days with
only a red diamond (L1) and no black bar (L2) did not pass V2 Level 2 cloud screening.
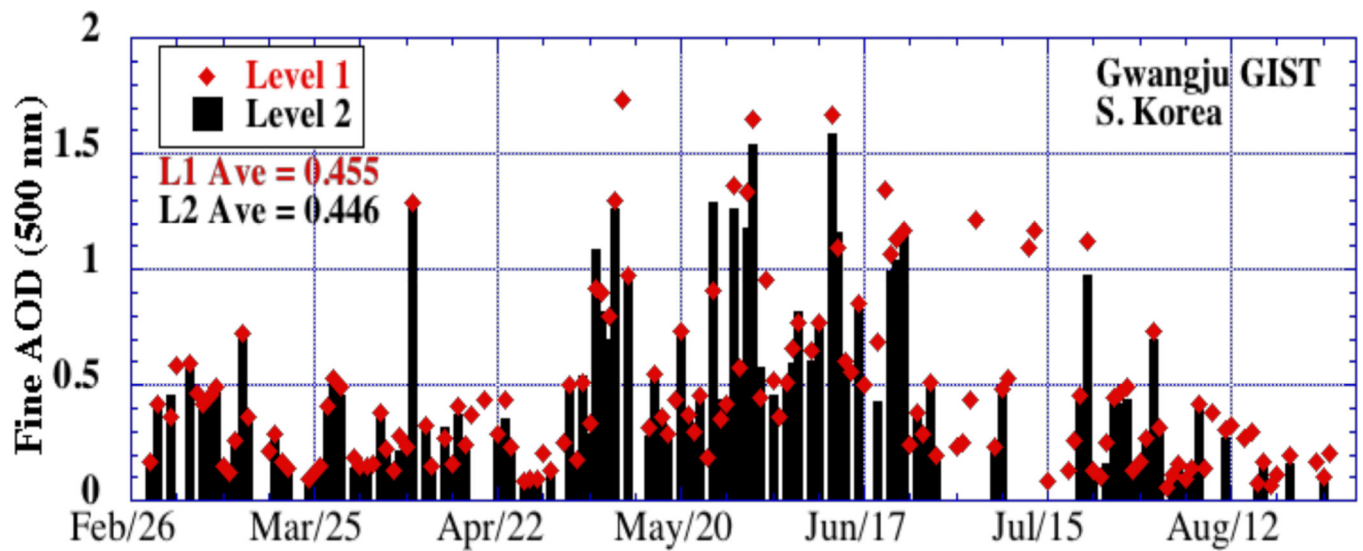
Figure 2.
Similar to Figure 1, the time series of daily averages of fine mode AOD at 500 nm (Version 2) retrieved from SDA for the AERONET site at Gwangju GIST, S. Korea. Note that cloud screening at times removes both high and low AOD days (see before and after July 15, for example), resulting in a similar time series average.
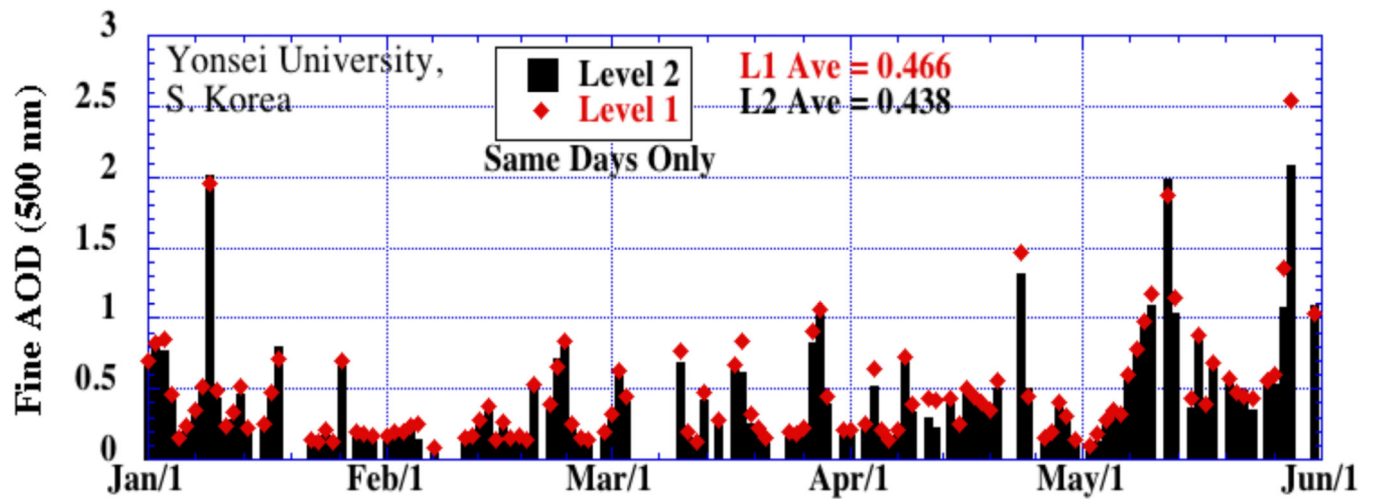
Figure 3.
Similar to Figure 1, the time series of daily averages of fine mode AOD at 500 nm (Version 2) retrieved from SDA for the AERONET site at Yonsei University, S. Korea, but only showing days that have passed L2 cloud screening.

DRAGON Korea Univ Site, Seoul, South Korea
May 27 - 31, 2012 SDA Fine and Coarse Mode AOD
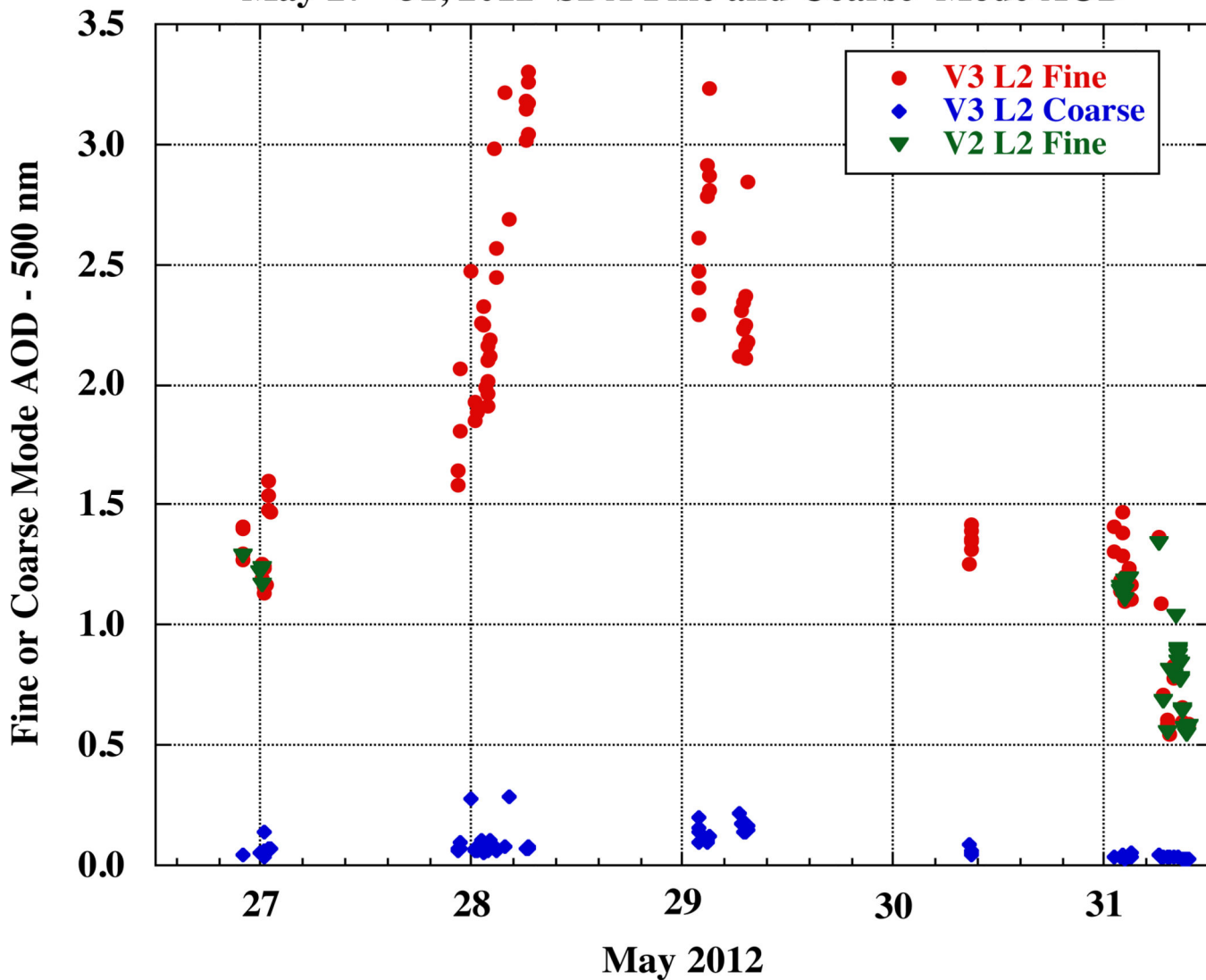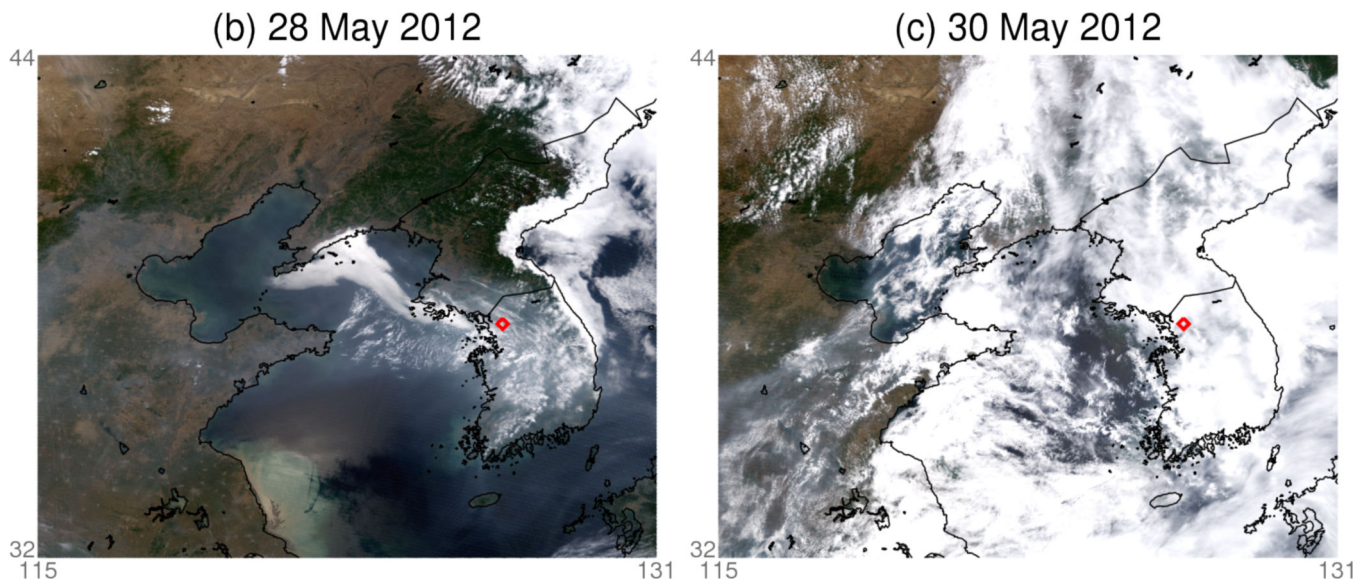
Figure 4.
(a) The time series from May 27–31, 2012 of instantaneous values of fine mode AOD at 500 nm retrieved from SDA for the AERONET site at Korea University, in Seoul S. Korea, showing cloud screened Version 2 data (green) plus Version 3 cloud screened fine (red) and coarse (blue) mode AOD. MODIS Terra images for May 28 and May 30 are shown in (b) and (c), with the Korea University site marked by a red diamond.
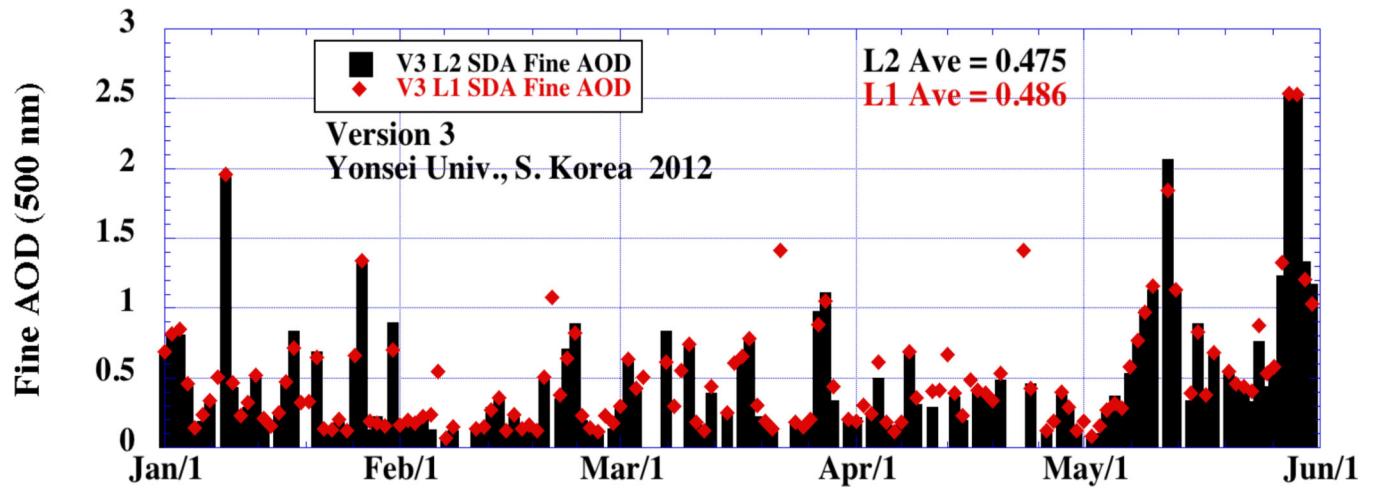
Figure 5.
Similar to Figure 1a, the time series of daily averages of fine mode AOD at 500 nm retrieved
from SDA for the AERONET site at Yonsei University, S. Korea, but for Version 3 cloud
and QA screening.
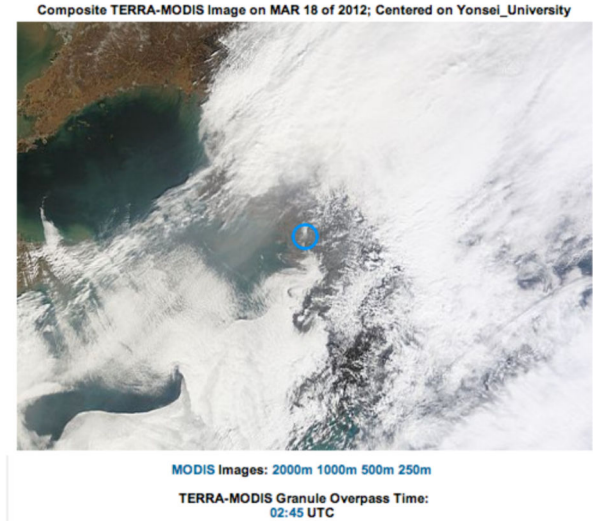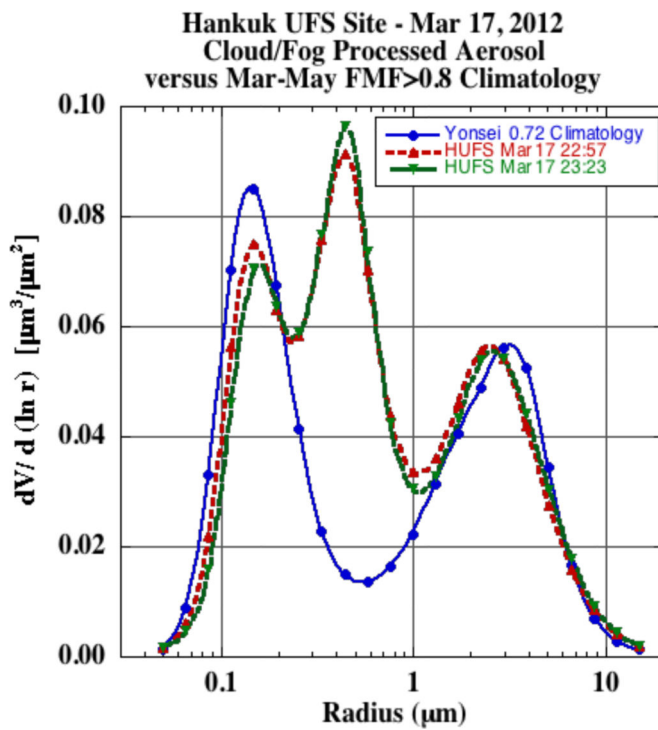
Figure 6.

(a.) Almucantar retrievals of aerosol size distributions from AERONET measurements made at the Hankuk UFS site on March 17, 2012, as compared to climatological mean size distributions from the Yonsei University site utilizing 42 retrievals from March through May 2011 and 2012 with average fine mode fraction (440 nm) of 0.88 and AOD(440nm) ranging from 0.6–0.8. (b.) MODIS Terra image from about 4 hours after the Hankuk UFS retrievals shown in (a). The blue circle indicates the Yonsei University site location.
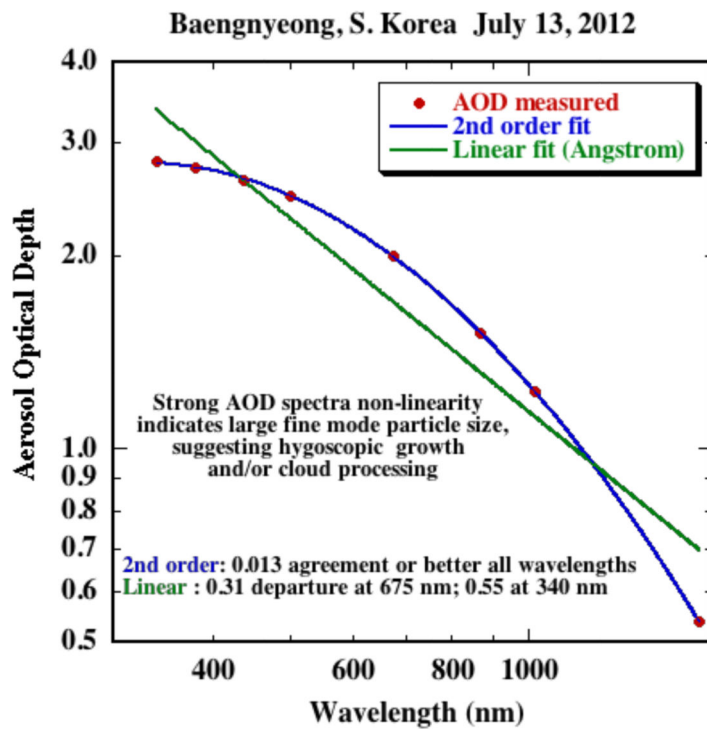
Figure 7.
(a.) Spectral AOD measurements at the Baengnyeong, S. Korea site on July 13, 2012, with linear and 2nd order regressions in logarithmic coordinates. (b.) MODIS Terra image from about one hour before the Baengnyeong AOD spectra shown in (a). The blue circle indicates the Yonsei University site location and the arrow shows the Baengnyeong site location.
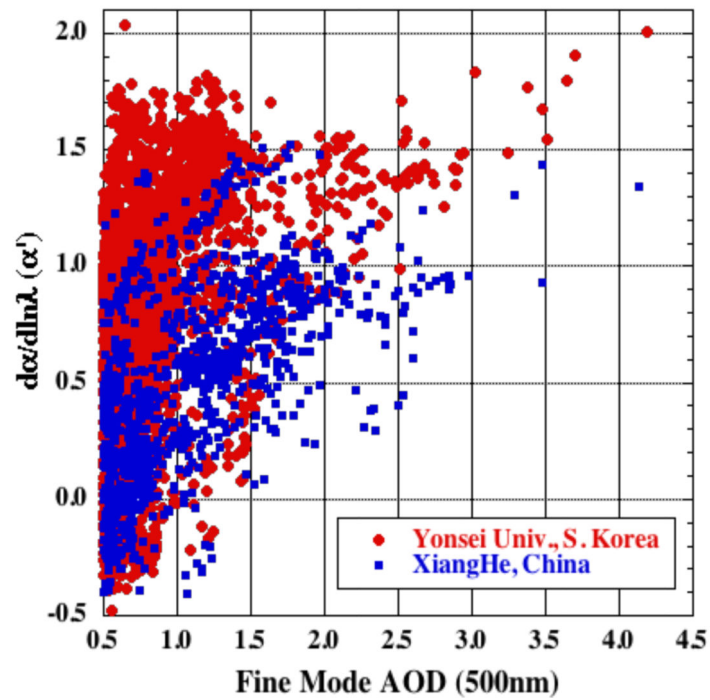
Figure 8.
Computations of the parameter dα/dlnλ(α') from instantaneous measurements of AOD
made at the Yonsei University and XiangHe AERONET sites from January 1 through May
31, 2012. This parameter is partly indicative of fine mode particle size, but also affected by
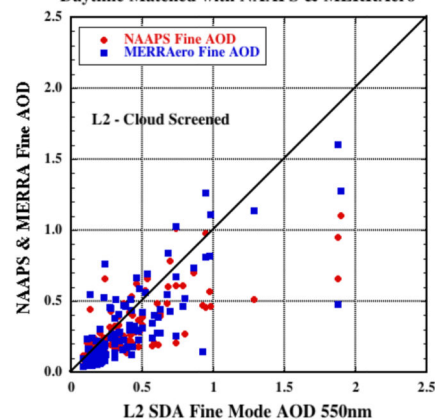coarse mode fraction of AOD.

Figure 9.
Time series of daily averages of AERONET Level 1 fine mode AOD at 550 nm (Version 2) retrieved from SDA from January 1 – June 1, 2012 for the AERONET site at XiangHe, China compared to MODIS Collection 6 satellite retrievals of total AOD from (a) Dark Target, (b) Deep Blue and (c) MAIAC algorithms.
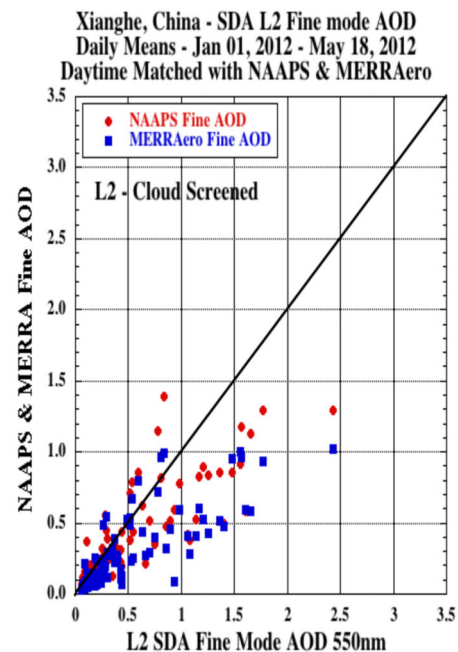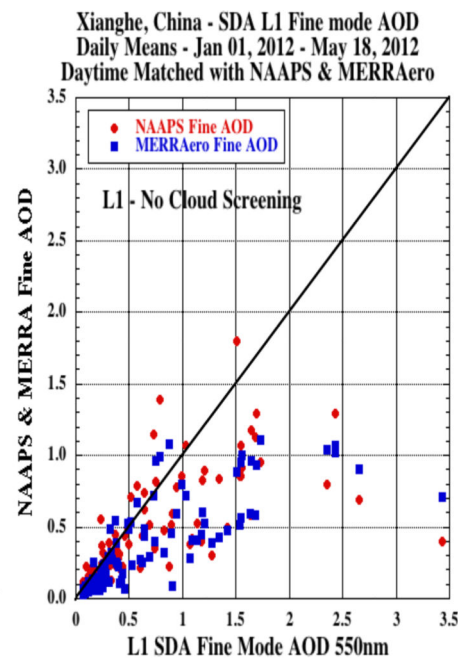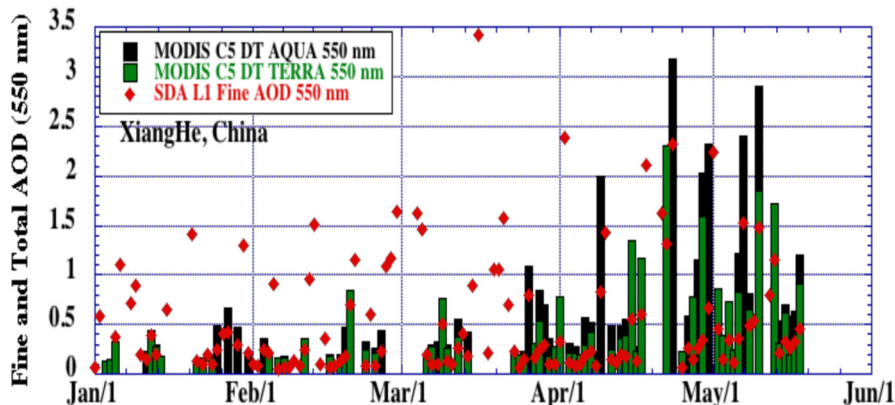
Figure 10 a-c.
(a) Time series of daily averages of AERONET Level 1 fine mode AOD at 550 nm (Version 2) retrieved from SDA from January 1 – June 1, 2012 for the AERONET site at XiangHe, China compared to MODIS Collection 5 satellite retrievals of total AOD from the Dark Target algorithm. (b) Scatterplot of NAAPS and MERRAero modeled daytime average fine mode AOD compared to AERONET L1 fine mode AOD daily averages. (c) same as plot (b) but for cloud screened L2 fine mode AOD from SDA.
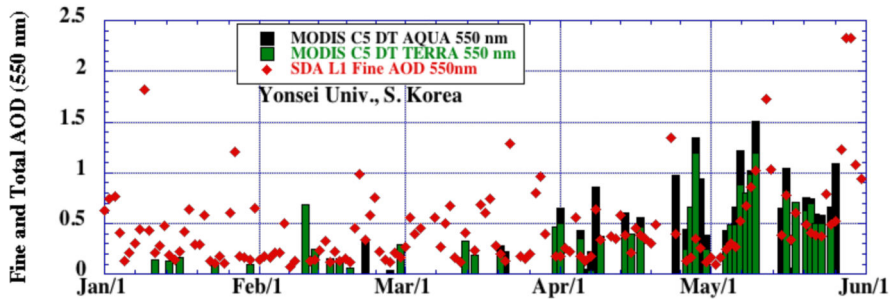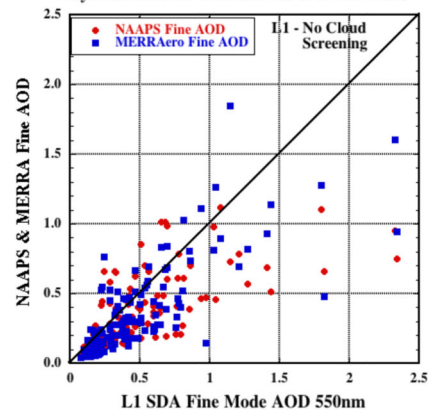
Figure 10 d-f.

(d) Time series of daily averages of AERONET Level 1 fine mode AOD at 550 nm (Version 2) retrieved from SDA from January 1 – June 1, 2012 for the AERONET site at Yonsei University compared to MODIS Collection 5 satellite retrievals of total AOD from the Dark Target algorithm. (e) Scatterplot of NAAPS and MERRAero modeled daytime average fine mode AOD compared to AERONET L1 fine mode AOD daily averages. (f) same as plot (e) but for cloud screened L2 fine mode AOD from SDA.
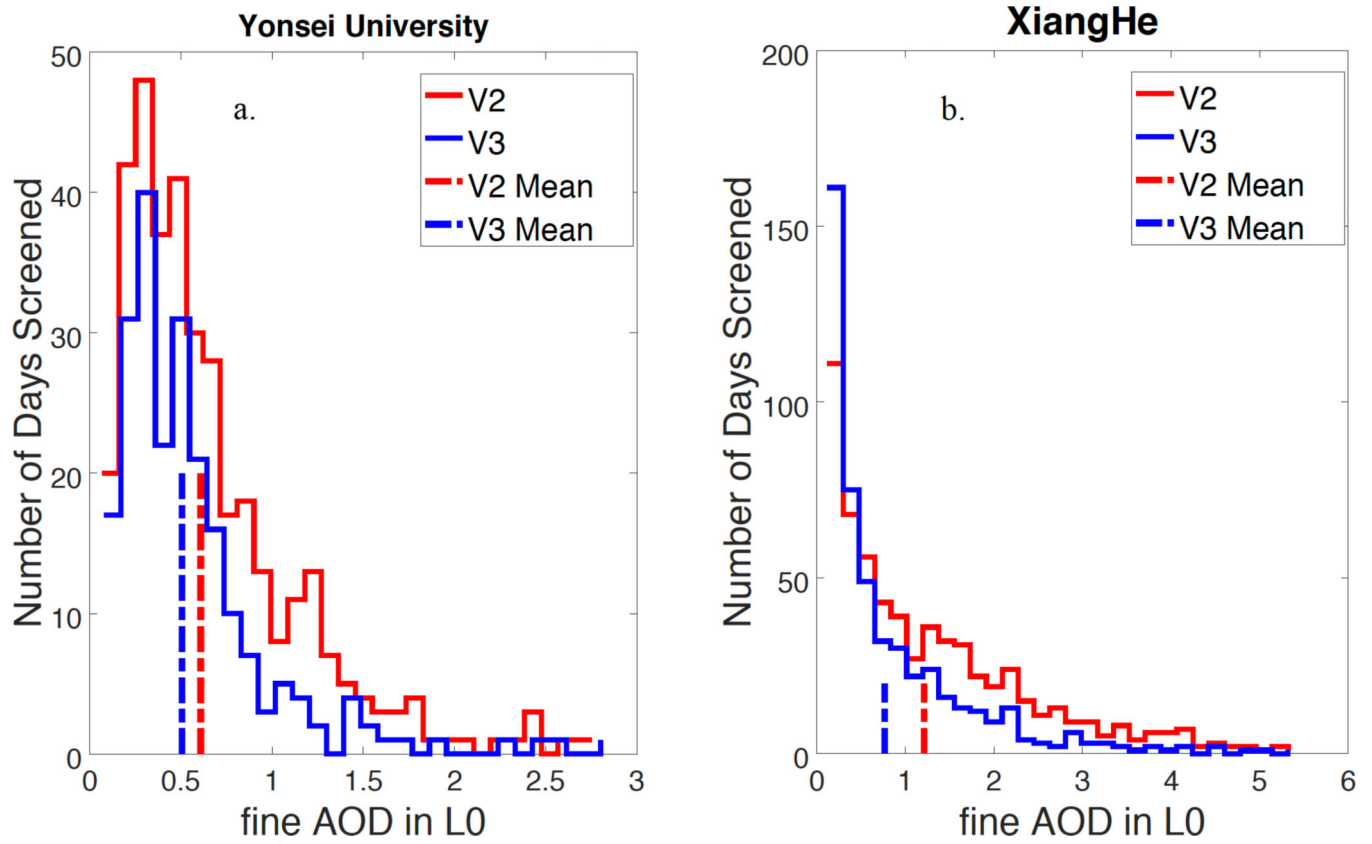
Figure 11.
The number of days eliminated (L1-L2=L0) as function of fine AOD bin by combined cloud
screening and data quality checks for both AERONET Version 2 data and the new Version 3
database, for the Yonsei University and XiangHe sites.

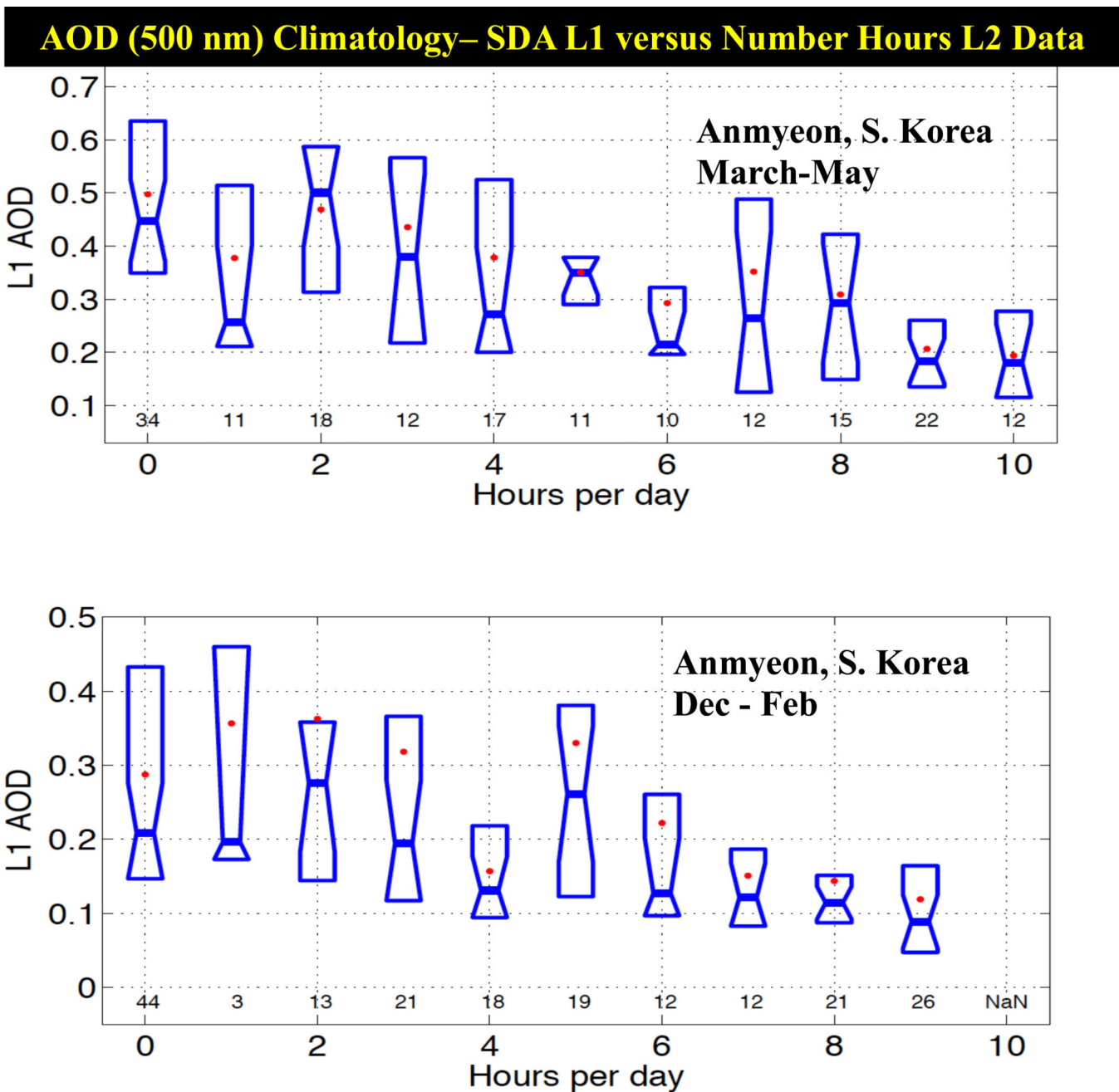**AOD (500 nm) Climatology– SDA L1 versus Number Hours L2 Data**
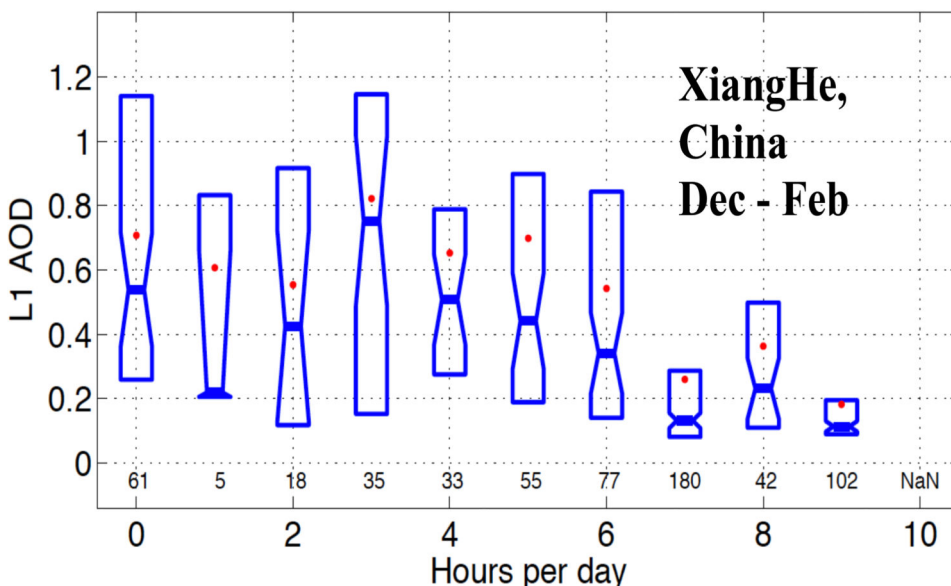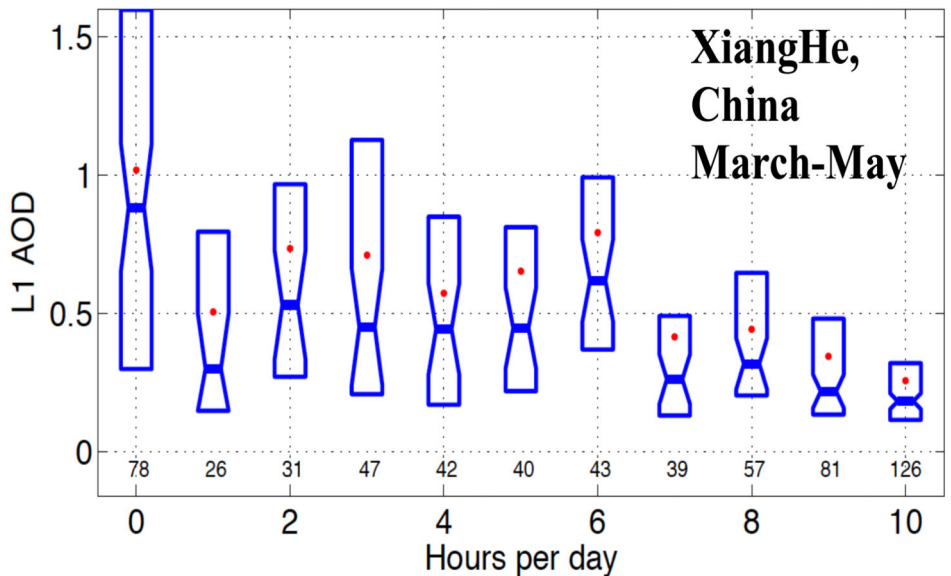
Figure 12a-d.
Level 1 (non-cloud screened) fine mode AOD (500 nm) from SDA versus number of hours per day of data that had passed Version 2 cloud screening (Level 2). Zero hours means that none of the L1 data passed the V2 cloud screening. The pinch point on the blue bars are the medians, the upper and lower limits of the blue bars represent the 75th and 25th percentiles. The red dots are the hourly means, and the numbers above the x-axis are the number of days of data for each hour-interval bin. Figures 12 a and b show climatological data for the XiangHe site for Spring and Winter seasons respectively, while Figures 12 c and d show the same for Anmyon.
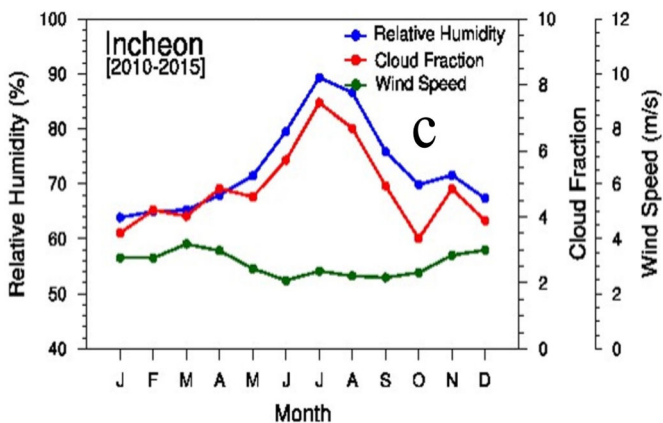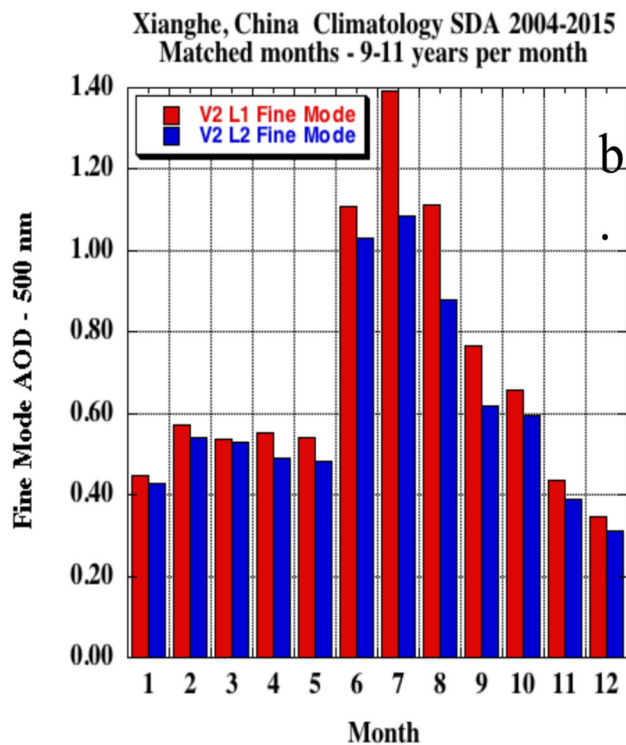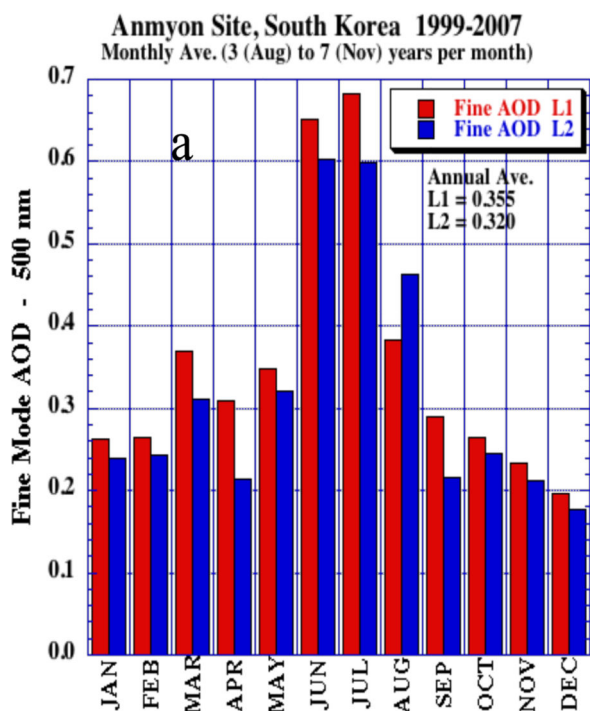
Figure 13.

(a.) Multi-year monthly mean fine mode AOD (500 nm; Version 2) from SDA, comparing cloud-screened (L2) to non cloud-screened (L1) data for the Anmyon site in S. Korea. **(b.)** Same as in a. but for the climatological means at the Xianghe site in China. (c.) Multi-year averages of cloud fraction, relative humidity and wind speed at the Inchon, S. Korea site ~110 km north of the Anmyon site.
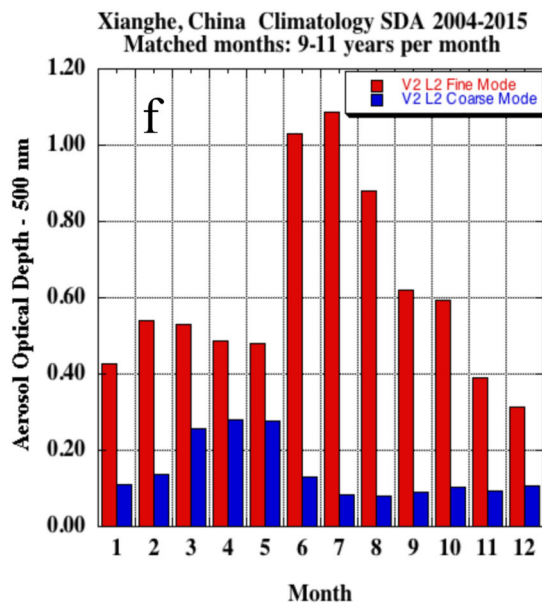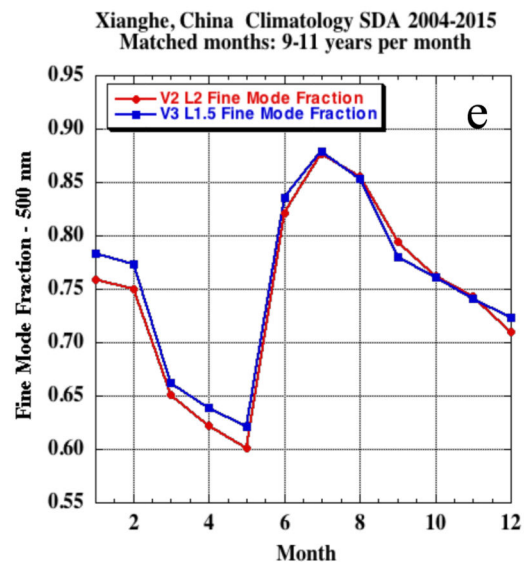
Figure 13.
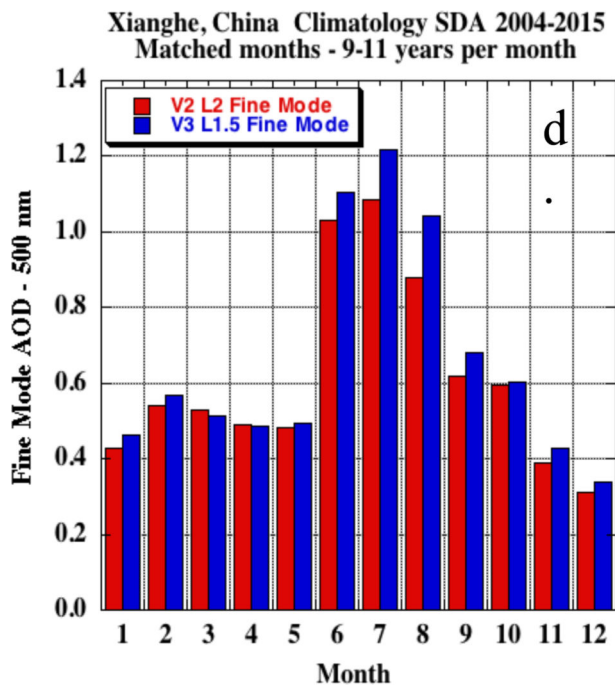(d.) Multi-year monthly mean fine mode AOD (500 nm) from SDA, comparing cloud-screened (L2) data from Version 2 to the newer Version 3 for the Xianghe site in China. (e.) Monthly means of the fine mode fraction of AOD (500 nm) comparing results from Version 2 to Version 3. (f.) Multi-year monthly mean fine mode and coarse mode AOD (500 nm) from SDA, from Version 2 cloud-screened (L2) data for the Xianghe site in China.

Table 1.

XiangHe,China Jan 1-May 18,2012 **SDA-Fine Mode** Daily Averages MODIS-Terra+Aqua **Days with AOD(550 nm) >0.8**

Retrieval	SDA fine L1	SDA fine L2	Dark Target	Deep Blue	MAIAC
#Days	32	22	12 (+8 dust*)	27 (+8 dust*)	25 (+4 dust*)
Days missed vs. L1 Fine Mode	N/A	12	24	14	13
% Missed vs. L1 (Fine AOD Days)		38%	75%	44%	41%
% Added Days - Non-Dust Days		6% (2 days)	12% (4 days)	28% (9 days)	19% (6 days)

*Dust days identified as >50% coarse Mode in SDA L2, and Fine AOD <0.8 in L1 & L2

#NOTE that DB and DT spatial resolution is 30 km radius and MAIAC is 61×61 km

Table 2.

In AERONET Version 2 data the Difference in number of days of daily average Fine Mode AOD (500 nm) in Level 1 (non-cloud screened) versus Level 2 (cloud screened) for different lower limits of AOD; Climatological data sets

Site Name	Days of L1	Days of L2	Days L1-L2	% Difference	AOD Lower Limit
XiangHe	3223	2703	520	16%	0
XiangHe	798	535	263	33%	1
Xianghe	264	138	126	48%	2
XiangHe	81	29	52	64%	3
XiangHe	25	5	20	80%	4
Yonsei Univ	1721	1370	351	20%	0
Yonsei Univ	164	101	63	38%	1
Yonsei Univ	14	5	9	64%	2

Table 3.

In AERONET Version 3 data the Difference in number of days of daily average Fine Mode AOD (500 nm) in Level 1 (non-cloud screened) versus Level 2 (cloud screened) for different lower limits of AOD; Climatological data sets

Site Name	Days of LI	Days of L2	Days L1-L2	% Difference	AOD Lower Limit
XiangHe	3222	2784	438	14%	0
XiangHe	796	672	124	16%	1
Xianghe	256	209	47	18%	2
XiangHe	79	61	18	23%	3
XiangHe	22	16	6	27%	4
Yonsei Univ	1718	1510	208	12%	0
Yonsei Univ	159	139	20	13%	1
Yonsei Univ	14	10	4	29%	2